Alteration at the base of the Siccar Point unconformity and further evidence for an alkaline provenance at Gale crater: Exploration of the Mount Sharp group, Greenheugh pediment cap rock contact with APXS

L. M. Thompson[1], J. G. Spray[1], C. O'Connell-Cooper[1], J. A. Berger[2], A. Yen[3], N. Boyd[4], R. Gellert[4], M. A. McCraig[4], and S. J. VanBommel[5]

[1]Planetary and Space Science Centre, University of New Brunswick, Fredericton, Canada

[2]NASA Johnson Space Center, Houston, USA

[3]Jet Propulsion Laboratory, California Institute of Technology, Pasadena, USA

[4] Department of Physics, University of Guelph, Ontario, Canada

[5]Department of Earth and Planetary Sciences, Washington University in St. Louis, St. Louis, USA

Corresponding author: Lucy Thompson (lthompso@unb.ca)

Key Points:

- Enhanced post-depositional fluid flow and alteration of the Mount Sharp group was focused at the Basal Siccar Point group unconformity
- Alkaline source rocks at Gale provided detritus to fluvial and eolian sandstones
- Bradbury and Siccar Point group sandstones may be contemporaneous, and younger than the Mount Sharp group

Abstract

Chemical data acquired by Curiosity's Alpha Particle X-ray Spectrometer (APXS) during examination of the contact between the upper Mount Sharp group and overlying Stimson formation sandstones at the Greenheugh pediment reveal compositional similarities to rocks encountered earlier in the mission. Mount Sharp group strata encountered below the Basal Siccar Point group unconformity at the base and top of the section, separated by >300 m in elevation, have distinct and related compositions. This indicates enhanced post-depositional fluid flow and alteration focused along this contact. Sandstone targets exposed immediately above the unconformity have basaltic compositions consistent with previously encountered eolian Stimson formation sandstones, except at the contact, where they show the addition of S. Resistant sandstone outcrops above the contact have higher K, Mn and Na and lower Ni concentrations that primarily reflect changes in provenance. They are compositionally related to cap rock float blocks encountered as Curiosity climbed through the Mount Sharp group, and Bradbury group sandstone outcrops. The higher K, pediment sandstones are interpreted to have a similar provenance to some Bradbury group sandstones, further evidence for widespread, alkaline source rock within and/or in the vicinity of Gale crater. The Bradbury and Siccar Point groups may both be younger than the Mount Sharp group. Alternatively, an alkaline source area in and around Gale crater has been eroded by both water and wind at different times (both before and after deposition of the Mount Sharp group), during the evolution of the crater and its infill.

Plain Language Summary

Chemical data acquired by Curiosity's Alpha Particle X-ray Spectrometer (APXS) during examination of an important regional contact between two rock units in Gale crater, Mars, reveal relationships with other rocks encountered much earlier in the mission. These relationships provide evidence for erosion by wind and water of various composition source rocks. These include more typical martian basaltic and more alkaline composition rocks (e.g., higher potassium and sodium). Distinct chemistry within rocks immediately underlying the contact, separated by more than 300 m in elevation, indicate enhanced fluid flow and alteration along the contact. These relationships provide important insights into regional and crater-scale processes and evidence for the long-lived role of water and aqueous alteration and hence, habitable environments at Gale.

1 Introduction

For the last two years, the Mars Science Laboratory (MSL) mission, *Curiosity* rover has been exploring a geomorphic trough on the lower slopes of Mount Sharp referred to as "Glen Torridon" by the MSL team. The trough overlaps with an area identified from orbit as clay-bearing (Anderson and Bell, 2010; Fraeman et al., 2016; Milliken et al., 2010; Thomson et al., 2011) and is delineated by Vera Rubin (formerly hematite) ridge (VRR) to the north and the Greenheugh pediment and sulfate-bearing unit to the south (also identified from orbit; Milliken

et al., 2014) (Figures 1, 2). Thus, this region potentially records the end of a "wetter" environment on Mars, before a transition to more arid conditions and deposition of the overlying sulfate-bearing strata. The region is therefore one of the primary exploration targets of the MSL mission (Anderson and Bell, 2010; Bibring et al., 2006; Fraeman et al., 2016, Milliken et al., 2010).

As part of the Glen Torridon campaign, *Curiosity's* traverse crossed the contact between the flat-lying strata of the Glen Torridon, clay-bearing unit and the overlying Greenheugh pediment-capping sandstones. The composition of the strata exposed either side of this contact was investigated using the Alpha Particle X-ray Spectrometer. This work documents the results of that investigation and discusses implications for the alteration history along the contact, and the provenance of the overlying capping sandstones.

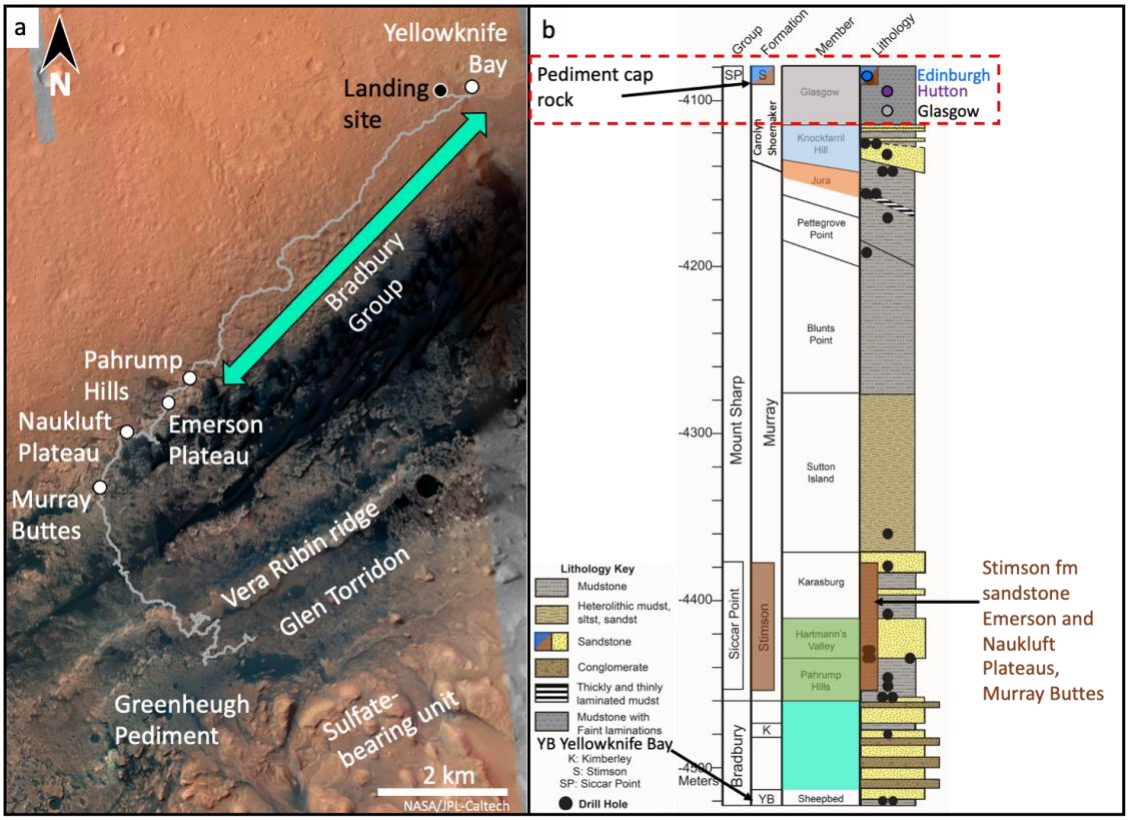

***Figure 1**. **a)** HiRise imagery with Curiosity's traverse to sol 2940, turquoise arrow shows the approximate extent of the Bradbury group; **b)** Stratigraphic column for the sedimentary strata encountered within Gale crater up to sol 2776.*

1.1 Geological background and context

The predominantly sedimentary strata encountered thus far on the mission have been divided into the Bradbury, Mount Sharp and Siccar Point stratigraphic groups (Figure 1b) (Banham et al., 2018; Fraeman et al., 2016; Grotzinger et al., 2015). The Bradbury group encompasses the interfingering lacustrine and fluvio-deltaic strata encountered from landing to arriving at the base of Mount Sharp (up to sol 722; Edgar et al., 2017, 2020; Grotzinger et al., 2014, 2015; Schieber et al., 2017; Williams et al., 2013). The Mount Sharp group comprises the Murray and Carolyn Shoemaker formations, which is in turn overlain by eolian sandstones of the Stimson formation, Siccar Point group (Figure 1b), (Banham et al., 2018, 2021; Fraeman et al., 2016).

The strata explored in Glen Torridon belongs to the upper Murray formation and the Carolyn Shoemaker formation (Figure 1b; Bennett et al., this issue). The Glen Torridon Murray formation is a continuation of the Jura member, first encountered on VRR (Fedo et al., 2020). The Jura member is overlain by the Knockfarril Hill and Glasgow members of the Carolyn Shoemaker formation. The Murray formation is characterized by lacustrine mudstones with minor intercalated sandstones (Edgar et al., 2020; Grotzinger et al., 2015; Stack et al., 2019). In contrast, the overlying Carolyn Shoemaker formation comprises more abundant fine sandstone preserving both cross-stratification and symmetrical ripples, as well as mudstone. This is interpreted to have been deposited at least in part, in a higher energy environment (Caravaca et al., this issue; Fedo et al., 2020). The Glasgow member immediately beneath the pediment and exposed on the upper reaches of Western butte is referred to as the Hutton interval, after the Hutton drill hole. It is characterized by a distinctly lighter tone, both from orbit and rover-based imagery (Bennett et al., this issue; Rudolf et al., this issue).

The rocks that cap the Greenheugh pediment comprise part of a more extensive, resistant, crater-retaining capping unit originally identified from orbit by Malin and Edgett (2000) who interepreted the unit to lie unconformably on the underlying strata. *Curiosity's* traverse confirmed the presence of an erosional unconformity between the Mount Sharp group and the overlying eolian Stimson formation, Siccar Point group at the Emerson and Naukluft plateaus and Murray buttes. This is referred to as the Basal Siccar Point group unconformity (Figure 1b, Banham et al., 2018, 2021; Fraeman et al., 2016). Mapping indicates that the unconformity drops in elevation ~140 m over a distance of ~2.3 km between these locations (Watkins et al., 2016).

Based on sedimentology and textures the Greenheugh pediment capping sandstones are interpreted to also belong to the eolian Stimson formation, Siccar Point group (Banham et al., this issue; Figure 1). They have been subdivided into intervals based on their sedimentology: the basal Gleann Beag interval (platy weathering), and the Ladder and Edinburgh intervals (characterized by their blockier, more massive appearance) (Banham et al., this issue). The basal surface of the pediment, like that of the Stimson formation previously encountered, is interpreted to represent the Basal Siccar Point group unconformity at this location (Banham et al., this issue; Bryk et al., 2019). It might also represent a weathering zone associated with what would have been eroded, exposed Mount Sharp group, prior to deposition of the sandstone. The unconformity may also have acted as a focus for later alteration and fluid flow in the underlying, less resistant Mount Sharp group. This follows deposition of the sandstones, as has previously been proposed for rocks encountered on VRR (Fraeman et al., 2020; Rampe et al., 2020a; Thompson et al., 2020).

1.2 APXS investigation of the Greenheugh pediment area

As part of the Glen Torridon campaign, *Curiosity* was able to drive up to the contact between the Mount Sharp group and the overlying Greenheugh pediment cap rock, and onto the pediment. (Bennett et al., this issue; Figures 1, 2). Obtaining compositional data at this location allows for comparison with the strata previously investigated along this important regional feature. It can help to assess the validity of the hypotheses outlined above. Specifically, elemental compositions measured by APXS can address questions such as:

1) Is the composition of the Mount Sharp group strata exposed at the contact with overlying cap rock in family with the rest of the Glen Torridon bedrock and Mount Sharp group, which might indicate enhanced alteration was not associated with the contact?

2) Or is there a distinct composition associated with the Mount Sharp group strata exposed along the contact with the pediment cap rock, indicating a greater degree of either weathering or alteration? If the chemistry is distinct, the changes in concentration of immobile versus mobile elements can shed light on the nature of the alteration process(es).

3) How does the composition of the Mount Sharp group at the Greenheugh, Basal Siccar Point group unconformity location compare to Mount Sharp group strata exposed at lower stratigraphic levels along the unconformity? A compositional relationship might indicate widespread weathering or alteration associated with the unconformity.

4) Do the Greenheugh pediment capping sandstones all have the same chemistry, or are there differences between the sedimentological intervals that might indicate changing provenance or physical transport/sorting/mixing processes? Distinct chemistry immediately at the unconformity might indicate alteration of the sandstone at the contact, or perhaps incorporation of underlying Mount Sharp group material.

5) How does the chemistry of the pediment capping sandstone compare to that of the Stimson formation sandstone encountered earlier in the mission? Do they have a related provenance? If there are differences in chemistry, do the Greenheugh capping sandstones show any compositional relationship to other sandstones analyzed by APXS during the course of the mission?

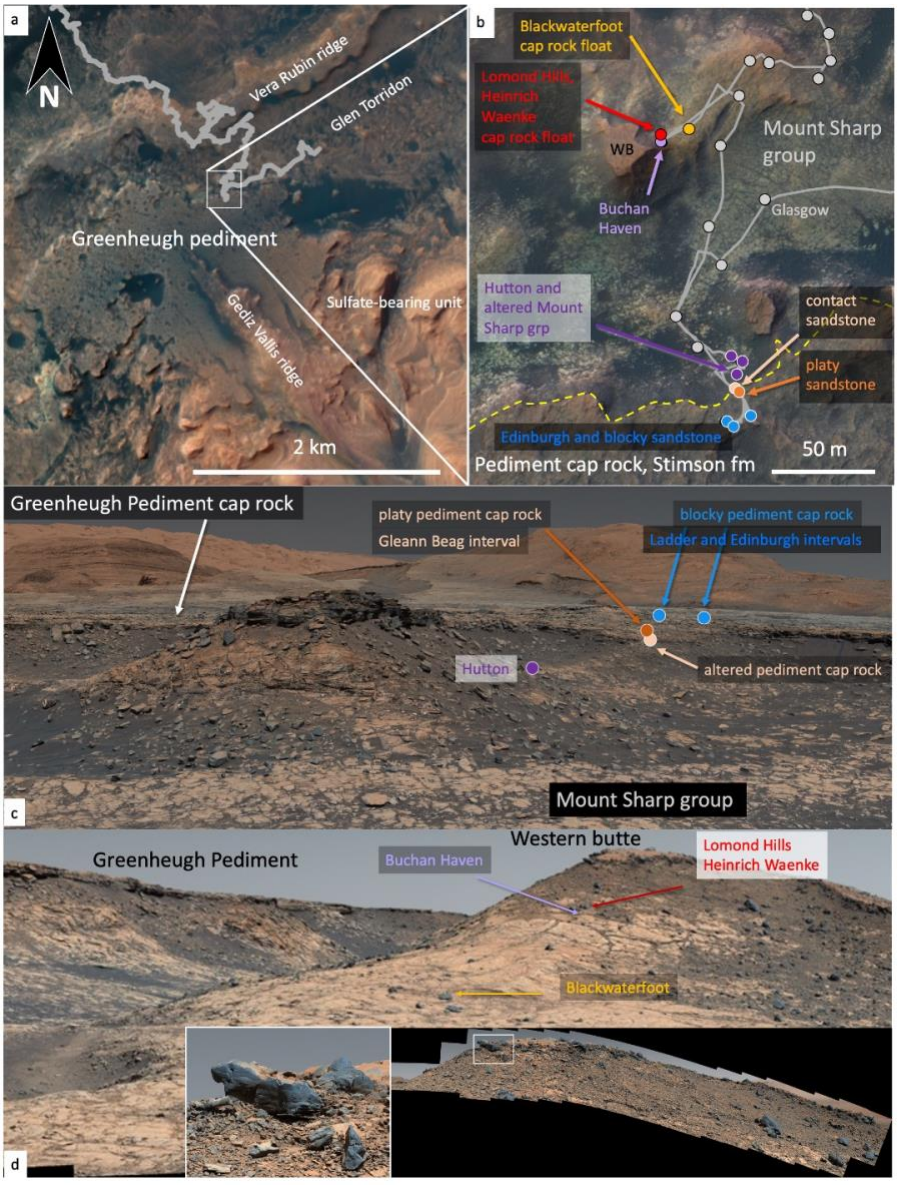

Figure 2. a) *Close-up HiRise with details of Curiosity's traverse, Vera Rubin ridge, Glen Torridon, the sulfate-bearing unit, Greenheugh pediment and Gediz Vallis ridge;* ***b)*** *HiRise with Curiosity's traverse overlain showing the area of interest (white box in a), Hutton interval targets, Glasgow, Greenheugh pediment capping sandstone targets, as well as cap float rock targets analyzed on Western butte (WB) encountered prior to ascending on to the pediment;* ***c)*** *Part of a Mastcam mosaic (sol 2633, mcam013796) looking towards the pediment and Mnt Sharp, showing location of APXS targets of interest*

2 Methods

2.1 Alpha Particle X-ray Spectrometer

The Canadian-built Alpha Particle X-ray Spectrometer (APXS) on *Curiosity* is the third iteration of APXS to fly on a Mars rover. The APXS is located on the end of *Curiosity's* robotic arm, which deploys the instrument to rock and soil targets. Particle induced X-ray emission and X-ray fluorescence techniques are used to induce characteristic X-rays within the sample (i.e., rocks and unconsolidated materials such as sand, soil and drilled samples). The X-rays produced by the sample of interest are detected by a silicon drift detector and the resulting spectrum used to determine composition. Further details of the APXS instrumentation, fundamentals, and calibration are provided by Berger et al. (2020), Campbell et al. (2012, 2014), Gellert et al. (2006, 2014), Reider et al. (2003) and VanBommel et al. (2016, 2017, 2019).

When placed in contact with the target of interest, APXS obtains analyses from a 1.5 cm diameter area. The area analyzed increases up to ~3.6 cm in diameter for a standoff of 2.5 cm from the target. The highest quality measurements (for Na, Mg, Al, Si, P, S, Cl, K, Ca, Ti, Cr, Mn, Fe, Ni, Zn and Br) are obtained when APXS is within 1 cm of the target, at the coldest time of day (overnight) and for integrations times >2-3 hours and typically 8 hours (e.g. VanBommel et al., 2019). Major element (and some minor element) chemistry of a target can be determined with high precision in as little as 10 minutes of integration time during the early morning or evening. Dusty targets can be brushed prior to APXS observations using the Dust Removal Tool (DRT; Davis et al., 2012).

APXS data are reported as weight percent (wt%) oxide except for Cl, which is reported as wt% element, and Ni, Zn and Br (and other trace elements), which are reported in µg/g (parts per

million - ppm). APXS does not determine oxidation state and therefore S, Cl, Mn and Fe are reported as SO_3, Cl, MnO and FeO respectively. Concentrations are normalized to 100%.

2.2 Other instrumentation utilized in this study

For the majority of targets analyzed by APXS accompanying high-resolution images are obtained. The Mastcam instrument provides context images of the workspace and surrounding area, while the Mars Hand Lens Imager (MAHLI) instrument typically acquires co-located, close-up images of the target of interest. See Edgett et al. (2012) and Malin et al. (2017) and for details of the MAHLI and Mastcam instruments respectively.

Powdered drill samples are delivered to *Curiosity's* internal Chemistry and Mineralogy (CheMin) and Sample Analysis at Mars (SAM) instruments. The CheMin instrument determines the mineralogy of a sample via X-ray diffraction (XRD, Blake et al., 2012), and the SAM instrument the organic and light element content via gas chromatography (GC), mass spectrometry (MS) and tunable laser spectrometry (TLS) (Mahaffy et al., 2012). Once the CheMin and SAM instruments have received sufficient sample, drill fines remaining in the drill bit assembly are dumped onto the ground and analyzed by APXS, along with any powdered material surrounding the drill hole, thus providing the bulk chemistry of related material ingested by CheMin and SAM.

2.3 APXS Sampling

The APXS-derived compositional characteristics of the Bradbury, Mount Sharp and Siccar Point groups encountered up to and including Vera Rubin ridge can be found in Berger et al. (2020) and Thompson et al. (2016, 2020). For a detailed summary of the chemistry of the Glen Torridon, Mount Sharp group, Murray and Carolyn Shoemaker formations as determined by APXS, see O'Connell-Cooper et al. (this issue).

Since the initial descent from VRR down into the Glen Torridon region, APXS has analyzed 153 rock, regolith and drill fines targets within the clay-bearing Mount Sharp group up to and including sol 2776 (sol – martian solar day, which equates to ~24 hours, 39 minutes and 35 seconds) (O'Connell-Cooper et al., this issue). Here we discuss in detail the Mount Sharp group, Glasgow member targets analyzed as we neared the Greenheugh pediment including the Hutton drill samples (Hutton interval, Bennett et al., this issue), as well as targets analyzed just after we left the pediment up to sol 2776, which include the Glasgow drill samples (Figure 2, Table 1a).

A further 22 APXS analyses were obtained on rock and drill fines (Edinburgh drill hole) associated with the Greenheugh pediment cap rock. These included 3 float rocks from a butte encountered prior to *Curiosity's* climb onto the pediment (i.e., Western butte) (Figure 2; Table 1b).

2.4 Treatment of the APXS data

Analyses with atypical alteration and diagenetic features or large veins (>0.5 cm) are distinguished from typical bedrock analyses. Atypical diagenetic and alteration features include irregularly distributed erosion resistant features, and different color patches and halos within the bedrock and associated with vein margins. Regolith analyses are excluded from the main Glen Torridon dataset.

Average, median, maximum and minimum, and 1σ standard deviation values are computed for: 1) the Mount Sharp group encountered prior to Glen Torridon, 2) Glen Torridon (GT) Jura and Knockfarril Hill member bedrock combined, 3) Glasgow member bedrock (excluding the targets within 3 m of cap rock, i.e., the Hutton interval), and 4) the Hutton interval (Table 1a).

Table 1. *APXS compositional data for* ***a)*** *the Mount Sharp group (grp) pre-Glen Torridon (GT); Glen Torridon, Mount Sharp grp Jura and Knockfarril Hill members (mbrs); Glasgow mbr including the Hutton interval and diagenetic features; and* ***b)*** *Stimson formation (fm) encountered at Emerson and Naukluft plateaus, and the pediment capping rocks. See supporting information for details. All data reported as wt% except Ni, Zn and Br (ppm).*

Table 1a		SiO_2	TiO_2	Al_2O_3	Cr_2O_3	FeO	MnO	MgO	CaO	Na_2O	K_2O	P_2O_5	SO_3	Cl	Ni	Zn	Br
Mount Sharp grp to GT	Average	48.31	1.04	9.29	0.32	18.53	0.22	5.56	4.40	2.55	0.89	0.96	6.40	1.21	870	1172	225
	Median	48.30	1.04	9.11	0.32	18.51	0.21	5.54	4.31	2.55	0.88	0.93	6.19	1.12	879	1084	125
n=302	Stdev	2.92	0.08	0.95	0.04	2.70	0.10	0.99	1.18	0.24	0.13	0.24	2.15	0.53	186	440	239
	Max	55.80	1.29	13.22	0.45	26.80	0.77	8.65	8.61	3.66	1.22	2.51	15.44	3.07	1832	2472	1396
	Min	41.05	0.79	7.22	0.24	9.13	0.06	2.66	2.08	1.99	0.58	0.48	1.85	0.30	231	397	14
GT Mount Sharp grp	Average	46.76	1.12	8.78	0.33	20.38	0.22	6.03	4.39	2.39	0.95	0.84	6.07	1.30	838	1936	541
Jura and Knockfarril Hill	Median	47.36	1.13	8.79	0.34	20.04	0.20	5.94	3.89	2.45	1.01	0.81	5.38	1.35	845	1631	479
mbrs	Stdev	3.21	0.06	0.62	0.03	1.67	0.12	0.92	1.70	0.23	0.21	0.14	2.70	0.38	116	1090	361
n=94	Max	53.17	1.30	10.17	0.40	26.24	0.61	8.06	9.98	2.73	1.36	1.35	16.19	2.12	1168	4411	1609
	Min	37.04	0.91	6.26	0.25	15.93	0.06	4.34	2.32	1.35	0.54	0.57	2.86	0.32	568	505	27
Glasgow mbr	Elevation/m																
Kirkcudbrightshire	-4118.12	45.29	1.14	8.53	0.36	18.42	0.22	7.65	5.22	2.52	0.72	0.93	7.32	1.32	840	1187	747
Stonehive	-4117.47	41.51	0.98	8.09	0.28	17.22	0.16	5.91	8.14	2.47	0.75	0.90	12.15	1.24	560	632	183
Upperhill_DRT	-4117.47	47.96	1.05	8.36	0.30	20.91	0.19	4.78	4.21	2.31	1.05	0.85	6.17	1.47	960	1037	1125
Glen_Mark	-4118.14	44.34	1.03	8.33	0.29	18.20	0.14	7.11	6.00	2.46	0.79	0.97	8.66	1.21	820	874	428
Conachair_DRT	-4119.31	47.26	1.15	8.77	0.38	18.27	0.20	7.09	4.76	2.32	0.78	0.89	6.54	1.16	892	1452	209
Conachair_offset	-4119.31	44.08	1.12	8.78	0.31	15.52	0.22	7.68	6.95	2.55	0.66	1.04	9.72	1.09	729	1210	84
Sourhope	-4118.12	46.37	1.11	8.84	0.33	18.26	0.21	6.30	4.95	2.40	0.85	0.93	7.98	1.20	857	1191	78
Gleneagles	-4119.31	45.65	1.05	8.17	0.32	20.15	0.17	6.40	4.79	2.40	0.95	0.80	7.61	1.10	1115	1340	573
Foggy_Moss	-4118.12	48.06	1.09	9.41	0.34	18.72	0.12	5.40	4.44	2.25	0.92	0.94	6.69	1.31	935	1175	128
Well_Run	-4119.19	47.98	1.03	9.10	0.26	19.38	0.18	5.73	4.19	2.38	0.94	1.03	6.37	1.11	890	1147	165
Staxigoe	-4117.94	48.25	1.19	8.99	0.38	17.87	0.15	6.45	4.19	2.64	0.87	0.81	6.37	1.46	895	1274	435
Scotnish_DRT	-4115.99	46.69	1.06	8.47	0.30	17.64	0.11	4.23	5.55	2.16	1.02	0.76	10.78	0.94	732	894	213
Renfrewshire	-4114.39	47.28	1.05	8.89	0.33	17.53	0.11	5.09	5.08	2.31	0.95	0.81	8.94	1.27	783	1287	19
Glenmard_Wood	-4110.72	44.21	1.07	8.93	0.33	20.12	0.19	6.76	5.13	2.51	0.62	0.81	7.88	1.14	1073	1074	122
North_Esk	-4109.56	45.74	0.99	8.64	0.28	17.75	0.12	6.17	5.85	2.51	0.66	0.80	8.99	1.05	848	781	189
Ben_Arnaboll_DRT	-4108.57	45.48	0.86	8.67	0.27	16.69	0.25	5.95	6.37	2.42	0.73	0.86	10.22	0.72	772	1332	178
Kennedys_Pass	-4109.26	48.86	1.01	9.05	0.25	18.61	0.13	5.87	4.12	2.38	0.78	0.98	6.39	1.30	838	810	356
Arbroath	-4109.49	49.86	1.00	9.42	0.34	16.93	0.10	5.75	3.94	2.61	0.84	0.88	6.63	1.25	910	984	54
Trossachs_DRT	-4109.49	50.02	1.08	8.86	0.31	18.27	0.14	4.98	3.93	2.68	0.88	0.92	5.86	1.71	898	946	1040
Sauchiehall_DRT	-4108.74	49.18	1.06	8.88	0.29	16.84	0.11	4.02	5.59	2.19	0.94	0.91	8.95	0.77	845	907	75
Rannoch_Moor	-4108.74	46.90	1.03	9.02	0.31	18.79	0.15	6.91	4.15	2.62	0.79	0.95	6.62	1.22	926	890	540
Marchmont	-4104.84	43.75	0.94	8.32	0.30	18.52	0.20	6.16	6.55	2.28	0.68	0.86	10.11	0.86	981	659	42
Cullivoe DRT	-4098.16	50.41	0.99	9.57	0.28	17.22	0.27	7.60	3.94	2.80	0.89	0.92	4.24	0.61	684	970	69
Glasgow1_tailings	-4107.93	47.51	1.10	8.69	0.41	19.02	0.22	4.71	6.22	2.11	0.78	1.05	6.99	0.91	916	876	29
Glasgow1_dump_corrected	-4107.93	46.87	1.08	8.74	0.38	18.82	0.17	4.74	6.11	2.23	0.91	1.03	7.48	1.12	964	1039	200
Glasgow_1_DRT	-4107.93	53.11	1.12	9.50	0.32	17.28	0.11	4.65	3.47	2.32	0.96	1.19	4.46	1.15	1080	1103	607
Glasgow_1_offset	-4107.93	48.32	1.00	8.73	0.29	15.98	0.11	4.76	5.79	2.33	0.86	1.03	9.16	1.27	913	972	494
Beefstand_Hill_DRT	-4105.43	50.95	1.04	9.51	0.29	19.14	0.15	4.31	3.71	2.37	0.88	0.99	5.82	0.58	828	935	74
Beefstand_Hill_offset	-4105.43	49.41	1.03	9.11	0.29	19.20	0.15	4.86	3.85	2.26	0.84	0.94	7.16	0.65	830	956	82
n=29	Average	47.29	1.05	8.84	0.31	18.18	0.16	5.79	5.08	2.41	0.84	0.92	7.66	1.11	873	1032	294
	Median	47.28	1.05	8.84	0.31	18.27	0.15	5.87	4.95	2.38	0.85	0.92	7.32	1.15	890	984	183
	Stdev	2.49	0.07	0.40	0.04	1.22	0.05	1.08	1.14	0.17	0.11	0.10	1.85	0.27	117	203	296
	Max	53.11	1.19	9.57	0.41	20.91	0.27	7.68	8.14	2.80	1.05	1.19	12.15	1.71	1115	1452	1125
	Min	41.51	0.86	8.09	0.25	15.52	0.10	4.02	3.47	2.11	0.62	0.76	4.24	0.58	560	632	19
Glasgow mbr, Hutton interval																	
Buchan_Haven_DRT	-4106.37	51.62	0.94	9.83	0.28	16.76	0.32	6.30	5.80	3.05	0.91	1.15	2.26	0.50	587	1547	89
Berwickshire_DRT	-4095.43	47.50	0.94	8.73	0.29	20.10	0.24	7.36	4.62	2.94	0.93	1.16	3.71	1.19	712	946	506
Cairnbulg	-4095.43	47.27	0.93	9.05	0.28	19.19	0.24	7.69	4.75	2.96	0.89	1.14	4.18	1.11	716	907	107
Hutton_DRT_centre	-4095.37	50.50	1.00	9.53	0.28	18.03	0.25	6.16	5.05	3.38	0.94	1.12	2.63	0.88	658	938	219
Hutton_dump_centre	-4095.37	49.29	1.07	9.27	0.28	18.68	0.26	5.39	6.10	3.51	0.93	1.04	2.99	0.91	716	1191	70
Hutton_dump_corrected	-4095.37	46.64	1.07	9.29	0.31	19.94	0.27	6.29	5.88	3.39	0.89	1.09	3.71	0.91	739	1598	131
Hutton_tailings	-4095.37	50.55	1.06	9.46	0.31	19.23	0.25	5.58	5.28	3.68	0.96	1.12	1.43	0.84	698	988	21
n=7	Average	49.05	1.00	9.31	0.29	18.85	0.26	6.40	5.35	3.27	0.92	1.12	2.99	0.91	689	1159	163
	Median	49.29	1.00	9.29	0.28	19.19	0.25	6.29	5.28	3.38	0.93	1.12	2.99	0.91	712	988	107
	Stdev	1.93	0.07	0.35	0.01	1.16	0.03	0.85	0.58	0.29	0.03	0.04	0.96	0.22	52	298	163
	Max	51.62	1.07	9.83	0.31	20.10	0.32	7.69	6.10	3.68	0.96	1.16	4.18	1.19	739	1598	506
	Min	46.64	0.93	8.73	0.28	16.76	0.24	5.39	4.62	2.94	0.89	1.04	1.43	0.50	587	907	21
Upper Glasgow mbr diagenetic features																	
Abernethy	-4106.37	24.55	0.43	5.20	0.08	40.12	5.11	7.53	3.59	1.66	0.21	0.69	8.55	1.81	560	2630	519
Moffat Hills	-4109.49	47.36	0.98	9.19	0.30	19.03	0.18	5.63	3.37	2.18	0.82	1.26	8.34	0.95	878	960	65
Bogmill_Pow	-4098.17	36.15	0.94	8.12	0.28	19.49	0.27	8.01	7.70	2.58	0.37	0.87	13.49	1.34	1153	1403	397
Liberton_Brae	-4095.37	40.60	0.85	7.62	0.25	16.25	0.25	17.11	3.31	1.86	2.14	0.97	6.67	1.42	1052	3433	486
Moorfoot_Hills	-4095.37	42.04	0.92	8.54	0.30	20.69	0.33	7.78	7.27	2.89	0.74	1.00	5.46	1.68	749	1097	765
Dunbartonshire_refined	-4095.37	26.38	0.58	5.09	0.14	39.65	6.33	8.57	3.60	1.57	0.24	0.62	4.89	1.97	893	1593	750
Dounreay	-4095.37	40.01	1.00	7.95	0.27	19.88	0.49	11.36	5.07	2.04	1.43	1.09	6.73	2.18	1283	1613	822

Table 1b		SiO_2	TiO_2	Al_2O_3	Cr_2O_3	FeO	MnO	MgO	CaO	Na_2O	K_2O	P_2O_5	SO_3	Cl	Ni	Zn	Br
Stimson fm from	Average	43.72	0.92	10.00	0.43	19.00	0.38	8.75	6.43	2.81	0.42	0.85	4.95	1.20	468	333	235
Emerson/	Median	43.66	0.92	9.46	0.42	19.23	0.39	8.76	6.51	2.76	0.43	0.87	5.24	1.19	448	314	194
Naukluft	Stdev	1.20	0.05	1.39	0.07	1.55	0.03	0.75	0.50	0.20	0.06	0.08	1.60	0.35	67	64	138
plateaus	Max	47.31	1.05	13.29	0.70	22.13	0.44	10.12	7.42	3.23	0.51	0.98	7.17	1.94	640	478	722
n=26	Min	41.63	0.81	8.18	0.33	14.80	0.29	6.88	4.98	2.56	0.29	0.72	0.65	0.61	386	217	76
Western butte float cap rock	Elevation/m																
Blackwaterfoot	-4108.57	44.42	0.77	9.16	0.63	19.13	0.48	8.74	7.25	3.22	1.21	0.90	3.23	0.74	293	373	57
Lomond_Hills	-4106.37	46.64	0.92	10.20	0.28	17.06	0.35	7.89	6.00	4.17	2.37	1.31	1.90	0.58	716	1367	74
Heinrich_Waenke	-4106.37	45.49	1.01	9.09	0.32	18.72	0.43	7.44	7.05	3.36	2.28	1.13	2.66	0.66	889	1876	38
Glaen Baeg interval (platy) cap rock																	
Huttons_Section	-4092.79	37.24	0.75	7.47	0.30	16.77	0.19	7.32	6.40	2.30	0.48	0.88	18.91	0.76	564	360	168
Clach_Glas	-4092.79	39.71	0.87	8.20	0.33	17.52	0.23	7.99	5.92	2.69	0.53	0.95	14.05	0.84	536	358	161
Galloway_Hills_DRT	-4091.75	41.72	1.00	8.58	0.56	21.05	0.46	9.91	6.37	2.65	0.39	0.86	5.11	1.18	593	465	60
Adder_raster3 (nodular)	-4090.90	41.52	0.95	8.97	0.39	19.83	0.41	9.43	6.59	2.78	0.45	0.93	6.54	1.05	560	448	46
Adder_raster2 (nodular)	-4090.90	42.03	0.97	8.77	0.42	20.08	0.42	9.28	6.47	2.80	0.44	0.92	6.06	1.17	567	448	73
Adder_raster1 (nodular)	-4090.90	40.99	0.92	8.92	0.42	19.13	0.40	9.65	6.40	2.76	0.46	0.89	7.65	1.24	545	419	53
Ladder and Edinburgh intervals (bocky) cap rock																	
Forsinard_Flows_offset	-4088.78	40.98	0.77	8.57	0.58	20.43	0.66	9.05	6.93	3.02	0.94	0.75	6.27	0.95	301	513	68
Forsinard_Flows	-4088.78	42.36	0.83	9.11	0.51	19.79	0.59	8.81	6.51	3.18	1.00	0.70	5.48	0.97	298	522	59
Machir_Bay_DRT	-4088.78	42.24	0.81	8.63	0.51	19.31	0.52	8.84	6.81	3.03	0.94	0.77	6.43	1.01	343	471	48
Edinburgh_dump_corrected	-4088.69	41.54	0.87	9.25	0.46	22.71	0.53	9.09	6.14	3.55	0.99	0.69	3.18	0.84	455	476	68
Edinburgh_tailings	-4088.69	39.54	0.87	8.86	0.42	22.67	0.54	9.36	7.10	3.45	1.09	0.59	4.58	0.81	408	353	77
Edinburgh_dump_2	-4088.69	41.85	0.92	9.36	0.40	21.25	0.49	8.58	6.23	3.29	0.96	0.69	4.79	1.04	387	407	56
Edinburgh_dump_1	-4088.69	41.70	0.83	9.22	0.45	20.10	0.52	8.44	6.25	3.05	0.81	0.84	6.37	1.17	390	375	50
Eshaness_DRT	-4088.69	39.18	0.84	8.22	0.55	21.58	0.56	9.25	6.36	3.08	0.84	0.64	7.18	1.61	357	331	93
Edinburgh_DRT	-4088.69	42.59	0.77	8.24	0.50	20.84	0.48	9.76	5.90	3.00	0.86	0.68	4.60	1.67	406	274	54
Edinburgh_offset	-4088.69	41.96	0.82	7.94	0.57	21.48	0.52	9.96	5.80	2.87	0.83	0.68	4.85	1.60	385	338	50
Assynt_Window_DRT	-4088.46	42.85	0.83	9.00	0.50	20.34	0.51	9.02	5.75	3.29	0.90	0.63	4.90	1.37	368	340	85
Glen_Feshie	-4088.46	40.98	0.90	8.82	0.46	20.53	0.51	8.71	6.34	3.15	0.89	0.76	6.49	1.33	345	329	32
All pediment cap rock	Average	41.22	0.87	8.68	0.46	20.27	0.47	9.01	6.36	2.97	0.75	0.78	6.86	1.14	443	404	72
(Gleann Beag, Ladder &	Median	41.70	0.87	8.78	0.46	20.34	0.51	9.05	6.37	3.02	0.84	0.76	6.27	1.09	406	407	60
Edinburgh intervals)	Min	37.24	0.75	7.47	0.30	16.77	0.19	7.32	5.75	2.30	0.39	0.59	3.18	0.76	298	274	32
	Max	42.85	1.00	9.36	0.58	22.71	0.66	9.96	7.10	3.55	1.09	0.95	18.91	1.67	601	522	168
	Stdev	1.40	0.07	0.49	0.08	1.48	0.11	0.66	0.37	0.32	0.24	0.12	3.65	0.27	104	70	36
Ladder & Edingburgh	Average	41.48	0.84	8.77	0.49	20.92	0.54	9.07	6.34	3.16	0.92	0.70	5.43	1.20	370	394	62
intervals only	Median	41.78	0.83	8.84	0.50	20.69	0.52	9.04	6.30	3.12	0.92	0.69	5.19	1.11	377	364	58
	Min	39.18	0.77	7.94	0.40	19.31	0.48	8.44	5.75	2.87	0.81	0.59	3.18	0.81	298	274	32
	Max	42.85	0.92	9.36	0.58	22.71	0.66	9.96	7.10	3.55	1.09	0.84	7.18	1.67	455	522	93
	Stdev	1.15	0.05	0.46	0.06	1.06	0.05	0.45	0.43	0.20	0.08	0.07	1.14	0.31	45	82	17
Gleann Beag interval only	Average	40.78	0.92	8.53	0.41	19.16	0.36	8.90	6.40	2.64	0.46	0.91	9.31	1.05	567	421	89
	Median	41.52	0.95	8.77	0.42	19.75	0.40	9.28	6.40	2.69	0.46	0.92	6.84	1.09	564	448	65
	Min	37.24	0.75	7.47	0.30	16.77	0.19	7.32	5.92	2.30	0.39	0.86	5.11	0.76	536	358	46
	Max	42.22	1.00	8.97	0.56	21.05	0.46	9.91	6.65	2.80	0.53	0.95	18.91	1.24	601	465	168
	Stdev	1.77	0.09	0.53	0.08	1.51	0.10	0.95	0.24	0.18	0.04	0.03	5.15	0.18	24	45	52

Average, median, maximum and minimum, and 1σ standard deviation values are also derived for: 1) the Stimson formation bedrock from the Emerson and Naukluft plateaus, 2) all Greenheugh pediment cap rock, 3) platy pediment cap rock only (Gleann Beag interval), and 4) blocky pediment cap rock (Ladder and Edinburgh intervals) (Table 1b).

All data is represented in various plots. See §S2.1, 2.3, 2.4, and 2.5 for details of plots. See Table S1 for a list of targets used in this study, Thompson (2022) for all derived data, and §S3 and S4 for relevant Mastcam and MAHLI images.

Statistical F- and t-tests were carried out to compare the variance and the difference/similarity of various subsets of the data (§S2.2, Tables S2 and S3). Relative increases and decreases in elemental concentrations were calculated for certain datasets, e.g., for the

Ladder and Edinburgh pediment capping sandstones relative to mean Stimson formation sandstone from the Emerson and Naukluft plateaus (§S2.7; Thompson 2022). Relative elemental gains and losses were also derived via a mass balance calculation for select datasets: 1) Hutton interval targets versus the Glasgow DRT target (typical Glasgow member bedrock and drill target), and 2) pediment cap rock diagenetic/alteration features versus the Galloway Hills pediment sandstone target within the Gleann Beag interval (§S2.7; Thompson 2022). The results of the mass balance and elemental increase/decrease calculations are represented graphically in the main body of the paper.

3 Results

3.1 Composition of the Hutton interval targets

The Mount Sharp group targets analyzed by APXS within 3 m of elevation of the pediment, referred to as the Hutton interval (Figures S2, S3, S8), are compositionally distinct for a number of elements from the rest of the Glen Torridon Mount Sharp group and most of the Mount Sharp group encountered prior to the Glen Torridon campaign (Figures 3a, b; Table 1a; Table S2). Hutton, Buchan Haven (Western butte) and other bedrock targets <3 m below the pediment have higher Na_2O concentrations (>2.94 wt%; 3.27 ± 0.29 wt%) than all other Glen Torridon rocks (2.39 ± 0.23 wt% GT Jura and Knockfarril Hill members; 2.41 ± 0.17 wt% Glasgow member), and most of the Mount Sharp group previously analyzed by APXS (2.55 ± 0.25 wt%). SO_3 is low (2.99 ± 0.96 wt%) compared to all bedrock targets encountered within Glen Torridon (6.07 ± 2.70 wt% GT Jura and Knockfarril Hill; 7.66 ± 1.85 wt% average Glasgow), and the Mount Sharp group preceding the campaign (6.40 ± 2.29 wt%). SO_3 does not correlate with CaO (R^2 = 0.08, R = -0.28), and the Hutton interval targets do not lie on a $CaSO_4$

addition trend line as is typical for the Mount Sharp group. Instead, the targets plot with excess Ca relative to the $CaSO_4$ addition trend line, indicating that the Ca is present in another phase (Figure 3c; Thompson et al., 2020).

The bedrock targets just below the pediment also trend to higher MnO and P_2O_5, and lower Ni (0.26 ± 0.03 wt%, 1.12 ± 0.04 wt%, 689 ± 52 ppm respectively) than the majority of other Glasgow member bedrock targets (0.16 ± 0.05 wt%, 0.92 ± 0.10 wt%, 873 ± 117 ppm respectively) (Figure 3a, b). They have the same characteristically low Zn concentrations as the rest of the Glasgow member (<1550 ppm) compared to the GT Jura and Knockfarril Hill members (≤4400 ppm) (Figure 3b). Unlike the rest of the Mount Sharp group, except for a number of Pahrump Hills member targets at the base of the section, Na correlates with Ti (R^2 = 0.8; Figure S1). The APXS bedrock targets with the most similar elemental trends are those encountered at the base of the Mount Sharp group, at Pahrump Hills, within the Pahrump Hills member, and a number of targets from the overlying Hartmann's Valley member (Figures 3a, c; Figure 1 for context). In particular, the Pahrump Hills member, Telegraph Peak and associated targets are the only other Mount Sharp group targets to exhibit the same significantly elevated Na as the Hutton interval (Figure 4a).

Mass balance calculations of the Hutton interval targets relative to the Glasgow DRT target (typical Glasgow member) reveal consistent and significant Na, Mg, Ca, Mn, and Fe gains, and losses of Ni. All the Hutton interval targets, with 2 exceptions, show loss of S, and all targets show less pronounced gains of K and Al (Figure 4b).

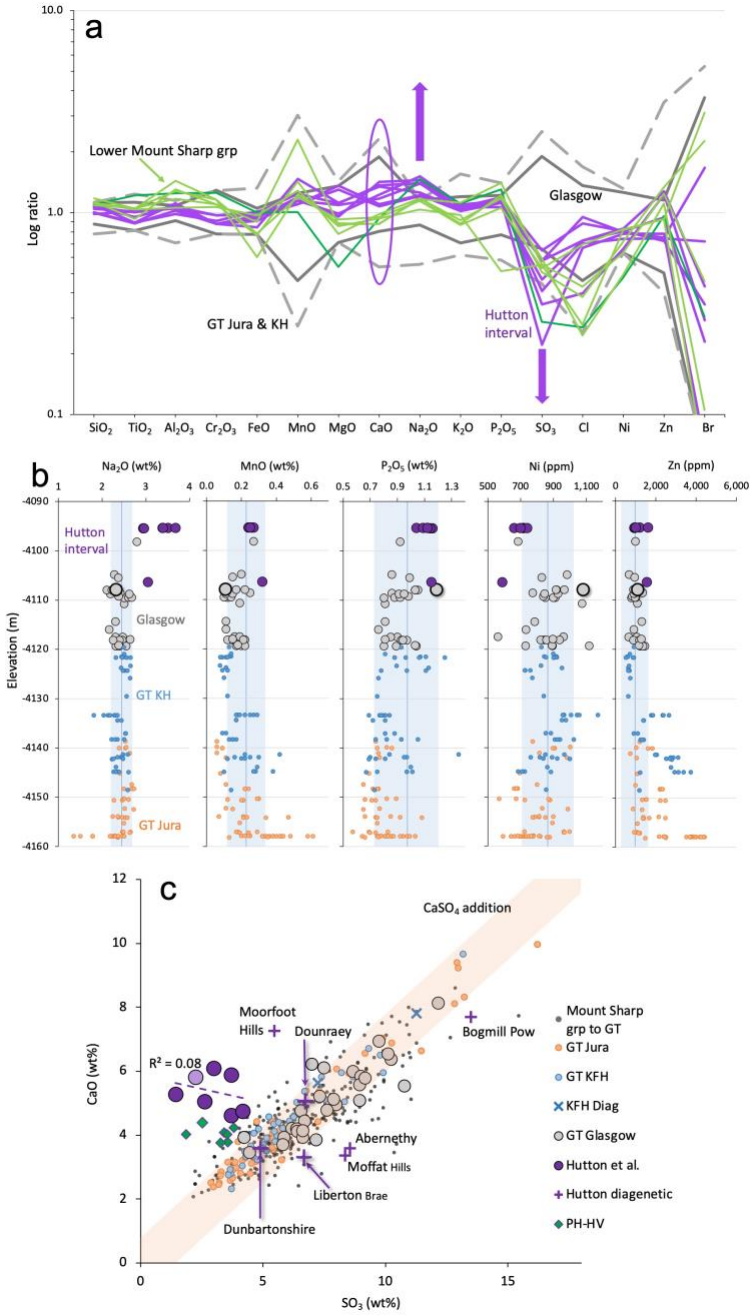

Figure 3. a) *Log ratio plot (relative to average Mount Sharp group (grp) pre Glen Torridon (GT)) showing the compositional range for GT Jura and Knockfarril Hill (KH) members (grey dashed lines), the range of Glasgow member compositions (solid grey lines), Hutton interval targets within 3 m of the pediment contact (purples), and lower Mount Sharp grp, Pahrump Hills and Hartmann's Valley member targets with similar elemental trends (greens). Note the elevated Na, and moderate Ca, but relatively low S associated with the Hutton interval targets, as well as many of the lower Mount Sharp grp targets;* ***b)*** *Select oxide and element concentrations for the GT Jura, Knockfarril Hill and Glasgow member targets plotted versus elevation (up to and including Glasgow drill fines; sol 2776). Hutton interval targets are in purple. Larger, thicker outlined Glasgow target is Glasgow DRT. Verical blue line indicates average Mount Sharp grp pre-GT, and the blue shaded area the 1σ standard deviation;* ***c)*** *CaO versus SO_3 plot for the Mount Sharp grp to GT, and the GT Jura, Knockfarril Hill and Glasgow members. Note that Hutton interval targets within 3 m of the pediment (purple), and the related Pahrump Hills and Hartmann's Valley targets (green diamonds) plot with excess CaO relative to the $CaSO_4$ addition trend line (orange)*

293

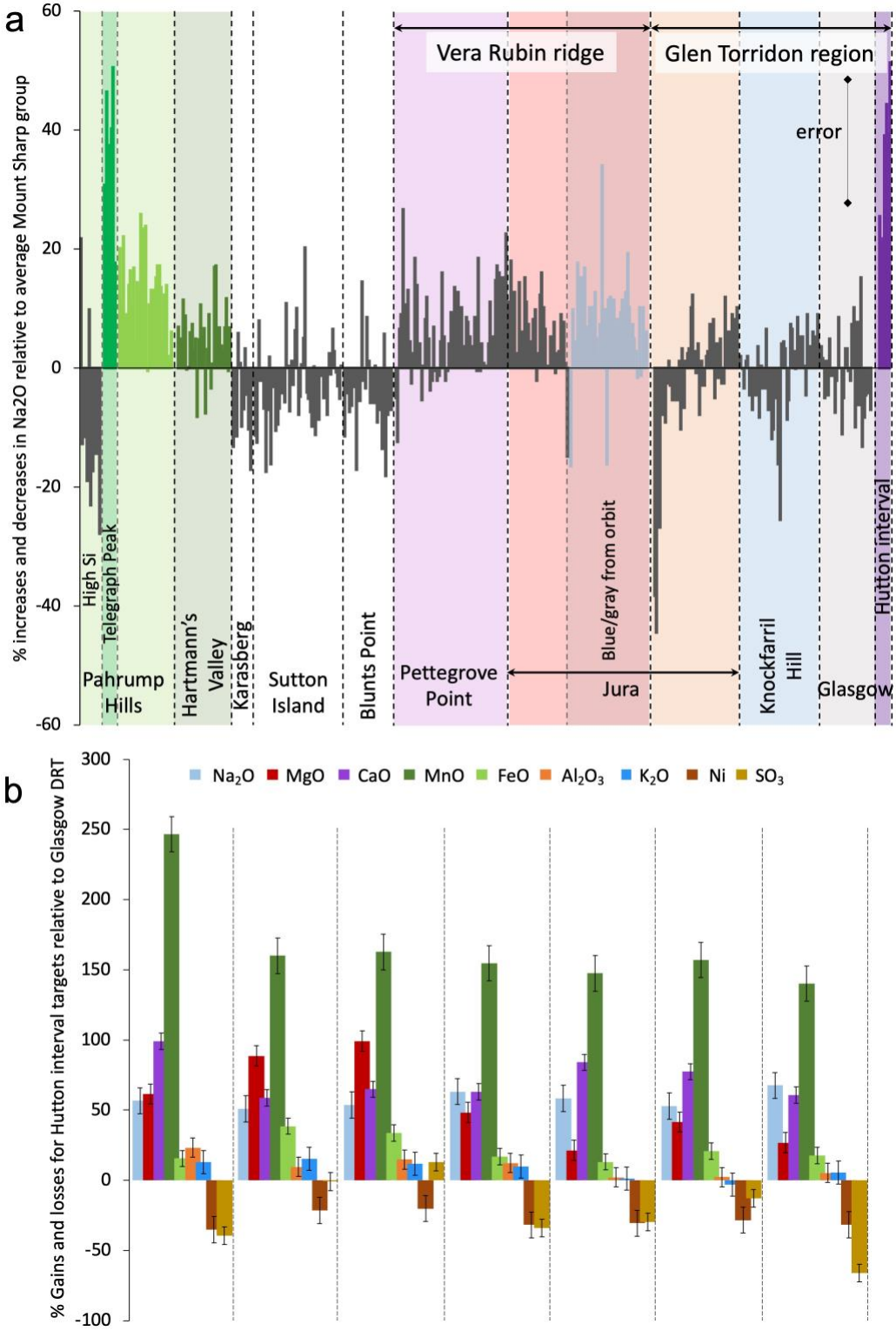

294
295 ***Figure 4a)*** *. %increases and decreases in Na_2O relative to average Mount Sharp group for the various members;* ***b)***
296 *Plot showing % gains and losses of Na, Mg, Ca, Mn, Fe, Al, K, Ni and S for Hutton interval targets compared to the*
297 *Glasgow DRT target (see §S2.8, Table S4)*

298 3.1.1. Diagenetic and vein targets

299 The number of features attributed to post-depositional, diagenetic processes observed
300 within the Glasgow member appeared to increase in abundance as *Curiosity* neared the
301 Greenheugh pediment (Bennett et al., this issue; Gasda et al., this issue). The bedrock itself
302 contains abundant, fine-scale (mm-size) resistant features. Larger-scale features analyzed by
303 APXS in the vicinity of the contact with the pediment capping rocks include; 1) Abernethy from
304 the Buchan Haven workspace, Western butte, 2) Moffat Hills and Bogmill Pow, and 3)
305 Dounraey, Liberton Brae and Moorfoot Hills, all from the Hutton drill workspace (Table 1a;
306 Figures S3, S10, S11 for images). Diagenetic target oxide and elemental abundances are log
307 ratioed to their respective bedrock target in the same workspace (Figure 5).

308 The Abernethy and Dunbartonshire targets, both darker toned and associated with cross-
309 cutting vein margins, are compositionally related, with comparable elemental trends relative to
310 their respective bedrock. Both exhibit very high FeO (40.12 and 39.65 wt% respectively) and
311 MnO (5.11 and 6.33 wt% respectively) concentrations. The Fe content is more than double, and
312 the Mn content is sixteen to twenty-four times that measured in the adjacent Buchan Haven and
313 Hutton bedrock targets (16.76 and 18.03 wt% FeO, and 0.32 and 0.25 wt% MnO respectively).
314 The Fe contents are among the highest concentrations measured by APXS at Gale and the Mn
315 concentrations are the highest.

316 Moffat Hills (resistant, knobbly textured with pits) has the same composition as the
317 nearby Trossachs bedrock target, but with slightly elevated P_2O_5 (1.26 wt% versus 0.92 wt%). It
318 plots with minor excess S relative to the typical Mount Sharp group $CaSO_4$ addition trend, as
319 does Abernethy (Figure 3c).

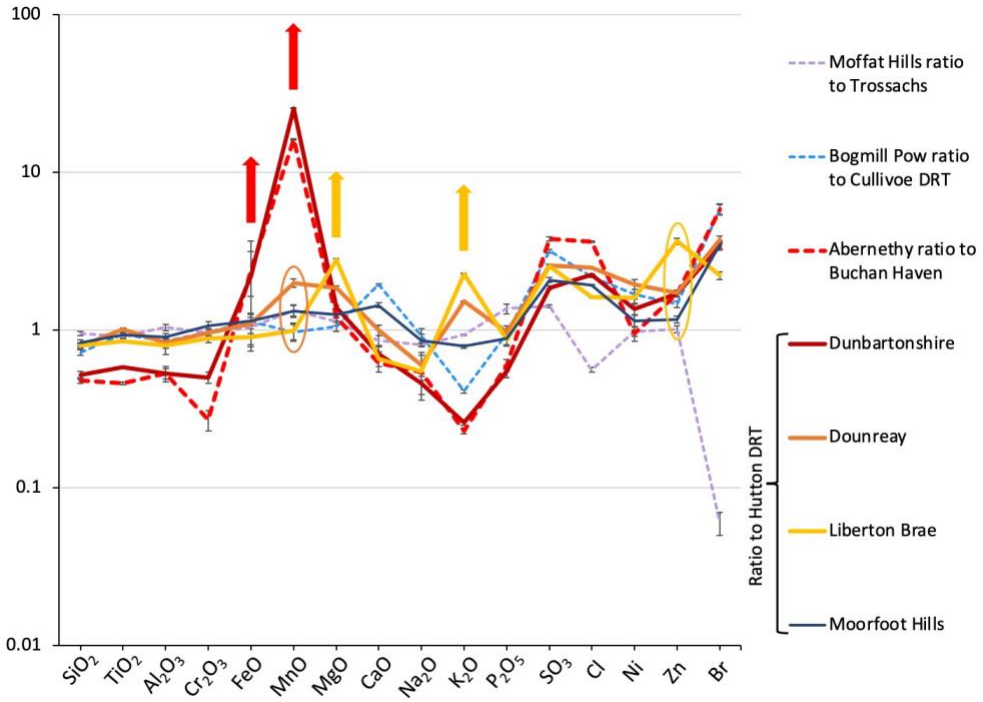

Figure 5: *Log ratio plot (relative to the bedrock target in the same workspace) showing relative increases and decreases in oxide and element concentrations of the diagenetic features analyzed in the upper Mount Sharp grp. Abernethy and Dunbartonshire (reds) both show very high Fe and Mn concentrations, and Dounreay and Liberton Brae (yellow/orange) exhibit elevated Mg and K.*

Bogmill Pow (fine-scale, spherical resistant features) and Moorfoot Hills (irregular shaped, resistant feature immediately adjacent to Liberton Brae) both have elevated Ca and S relative to the bedrock in the same workspace, consistent with the addition of ~15 and 4 wt% $CaSO_4$ respectively (Figure 3c). Moorfoot Hills plots off the general $CaSO_4$ addition trend line, but is consistent with the addition of $CaSO_4$ to the respective Hutton bedrock target, which also plots with excess Ca relative to other Mount Sharp bedrock (Figure 3c). Other elements are diluted except Mg, Cl, Mn, Fe, Ni, and Zn (Figure 5).

The Liberton Brae and Dounraey features are both light-toned, resistant and smooth compared to the bedrock and are associated with the same vein as the Dunbartonshire and Moorfoot Hills features. They both exhibit elevated MgO and K_2O (17.11 and 11.36 wt% MgO,

and 2.14 and 1.43 wt% K_2O respectively) relative to the bedrock. Liberton Brae also has elevated Zn, and Dounraey somewhat elevated Mn (Figure 5).

3.2 Composition of the Greenheugh pediment cap rocks

3.2.1. Previous Stimson formation APXS results

Outcrops of Stimson formation sandstone were first encountered in the vicinity of Pahrump Hills on the Emerson and Naukluft plateaus (Figure 1) and analyzed by APXS between sols 998 and 1351. Stimson formation sandstone exposures were also imaged at Murray buttes, but not analyzed by APXS. The Emerson and Naukluft plateaus are separated by more than 3.5 km lateral distance from the Greenheugh pediment. The Stimson formation is interpreted to represent lithified, basaltic, Mars soil-like composition, eolian sand (Banham et al., 2018, 2021; Thompson et al., 2016; Yen et al., 2017), which has undergone predominantly isochemical alteration (Hausrath et al ., 2019; Yen et al., 2017). The exception are targets associated with silica-rich alteration haloes (Yen et al., 2017). We refer to the basaltic, martian sand/soil composition of the Stimson targets encountered at Emerson and Naukluft plateaus as "typical Stimson" (Table 1b). Owing to the soil-like composition of the Emerson/Naukluft plateau Stimson sandstones, we use Lagrange (typical Gale soil, sol 605) as a comparison target in ratio plots (Figure 6) . However, we demonstrate below that not all rocks grouped as Stimson formation based on sedimentological observations conform to typical Stimson, basaltic compositions.

3.2.2. Gleann Beag interval (platy)

The two pediment cap rock targets exposed immediately at the contact with the underlying Mount Sharp group (Figures S4, S12) are characterized by elevated S (14.05 and

18.91 wt% SO_3) relative to typical Stimson formation sandstones (0.65 – 7.17 wt% SO_3) and the overlying sandstones (5.11 – 7.65 wt% SO_3) (Table 1b, Figure 6a, 7). The increased S content does not correlate with an increase in Ca (Figure 6a, 7), and therefore cannot be attributed to any appreciable $CaSO_4$ content. The majority of other elements are diluted relative to typical Stimson formation and the overlying Gleann Beag sandstones, except K, P, and Ni (Figure 6a).

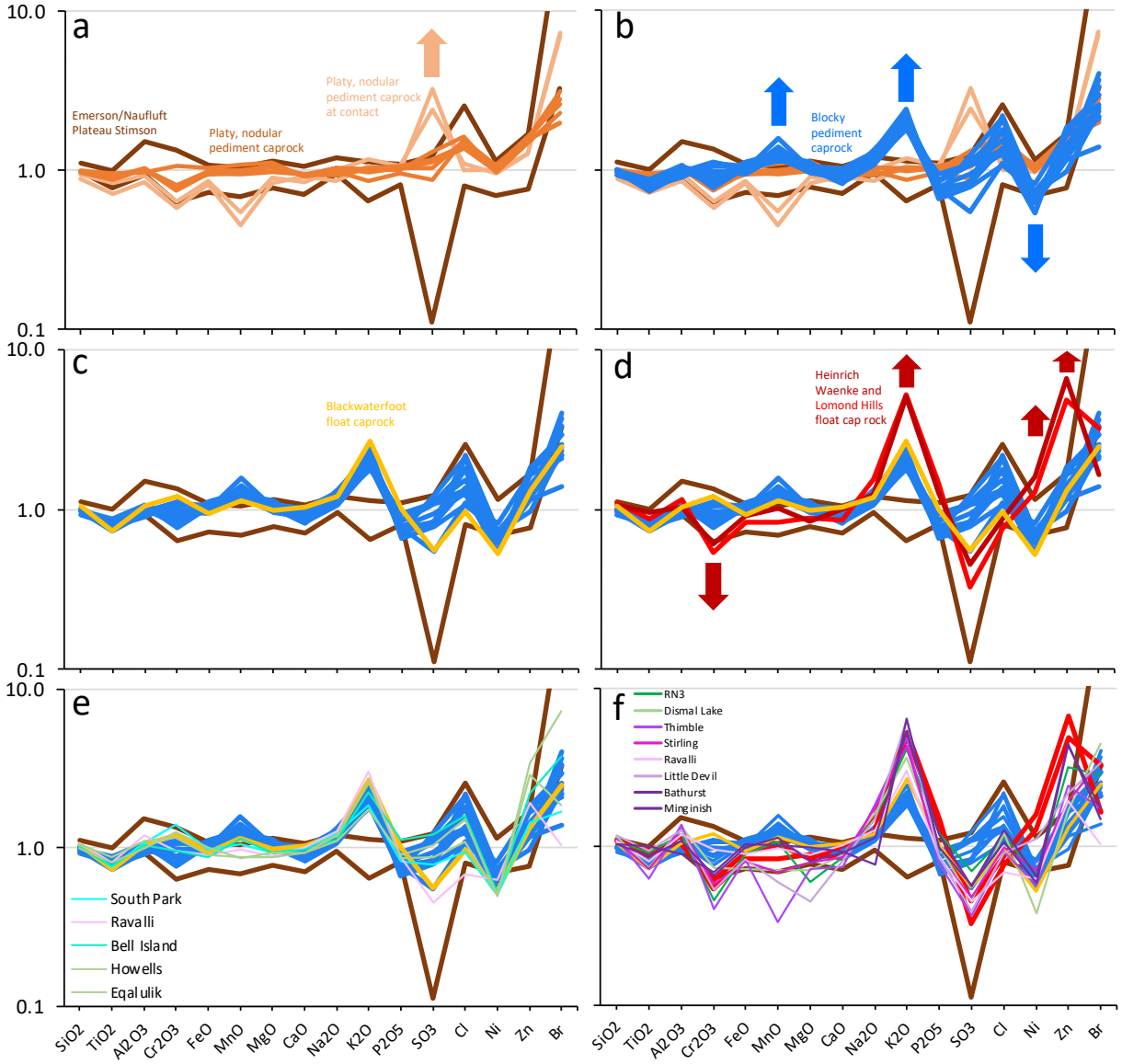

Figure 6: *Log ratio plots (relative to Lagrange, typical Gale soil target from sol 605) with the compositional range of typical Stimson sandstone APXS targets from the Naukluft and Emerson plateaus (brown lines) and a) capping sandstones at the pediment contact (oranges), lighter orange elemental traces are the two targets analyzed immediately at the contact; b) showing the addition of pediment capping sandstones analyzed higher up the section from the Ladder and Edinburgh intervals (blue); c) Ladder and Edinburgh interval sandstones and Blackwaterfoot*

float cap rock (yellow); d) with the addition of Lomond Hills and Heinrich Waenke float cap rocks (red); e) compositionally related targets to the Ladder and Edinburgh interval sandstones encountered earlier in the mission; and f) compositionally related targets to Lomond Hills and Heinrich Waenke encountered earlier in the mission (RN3 – Rocknest 3).

The Gleann Beag interval cap rock sandstones above the high S contact (Figures S5, S13) fall within the same compositional range as typical Stimson formation sandstone (Table 1b; Figure 1, 6a). Nodule rich areas (Adder targets, Figure S13) have the same composition as the more nodule-free bedrock (Galloway Hills) (Table 1b; Figure 6a). The platy, Gleann Beag sandstones are statistically, compositionally the same as typical Stimson sandstones except for Si, Al, P, Ni, and Zn (see results of t-tests, Table S3). While the Si, Al, P, Ni, and Zn concentrations are statistically distinct, Gleann Beag interval concentrations overlap with typical Stimson for all five elements (Table 1b, Figures 6a, 7).

3.2.3. Ladder and Edinburgh intervals (blocky)

In contrast to the sandstones analyzed at the contact, more resistant sandstones exposed higher up the section within the Ladder and Edinburgh intervals weather in a blockier fashion (Figures S6, S7, S14) and have distinct compositions as illustrated in Figures 6b, 7, and 8. T-tests reveal that the blocky sandstones are statistically different than the typical Stimson for every element except Mg, Ca, S, and Cl (Table S3).

The Ladder and Edinburgh sandstones have significantly increased (up to 2.6 times) K_2O concentrations (0.92 ± 0.08 wt%) compared to typical Stimson formation sandstones (0.42 ± 0.06 wt%) and the platy pediment cap rock exposed within the Gleann Beag interval (0.46 ± 0.04 wt%). MnO concentrations are also elevated (0.54 ± 0.05 wt%) within the Ladder and Edinburgh interval compared to typical Stimson (0.38 ± 0.03) and the Gleann Beag interval (0.36 ± 0.10). The Ladder and Edinburgh sandstones also trend to higher Na_2O (3.16 ± 0.20 wt%), FeO (20.92 ± 1.06 wt%), and Cr_2O_3 (0.49 ± 0.06 wt%) concentrations compared to typical Stimson

formation sandstones (2.81 ± 0.20 wt% Na_2O, 19.00 ± 1.55 wt% FeO, 0.43 ± 0.07 wt% Cr_2O_3) and Gleann Beag sandstones (2.64 ± 0.18 wt% Na_2O, 19.16 ± 1.51 wt% FeO, 0.41 ± 0.08 wt% Cr_2O_3). They are also characaterized by lower TiO_2, P_2O_5, and Ni concentrations (0.84 ± 0.05 wt%, 0.70 ± 0.07 wt% and 370 ± 45 ppm respectively) than Stimson (0.92 ± 0.05 wt%, 0.85 ± 0.08 wt% and 468 ± 67 ppm respectively) and Gleann Beag sandstones (0.92 ± 0.09 wt%, 0.91 ± 0.03 wt% and 567 ± 24 ppm respectively).

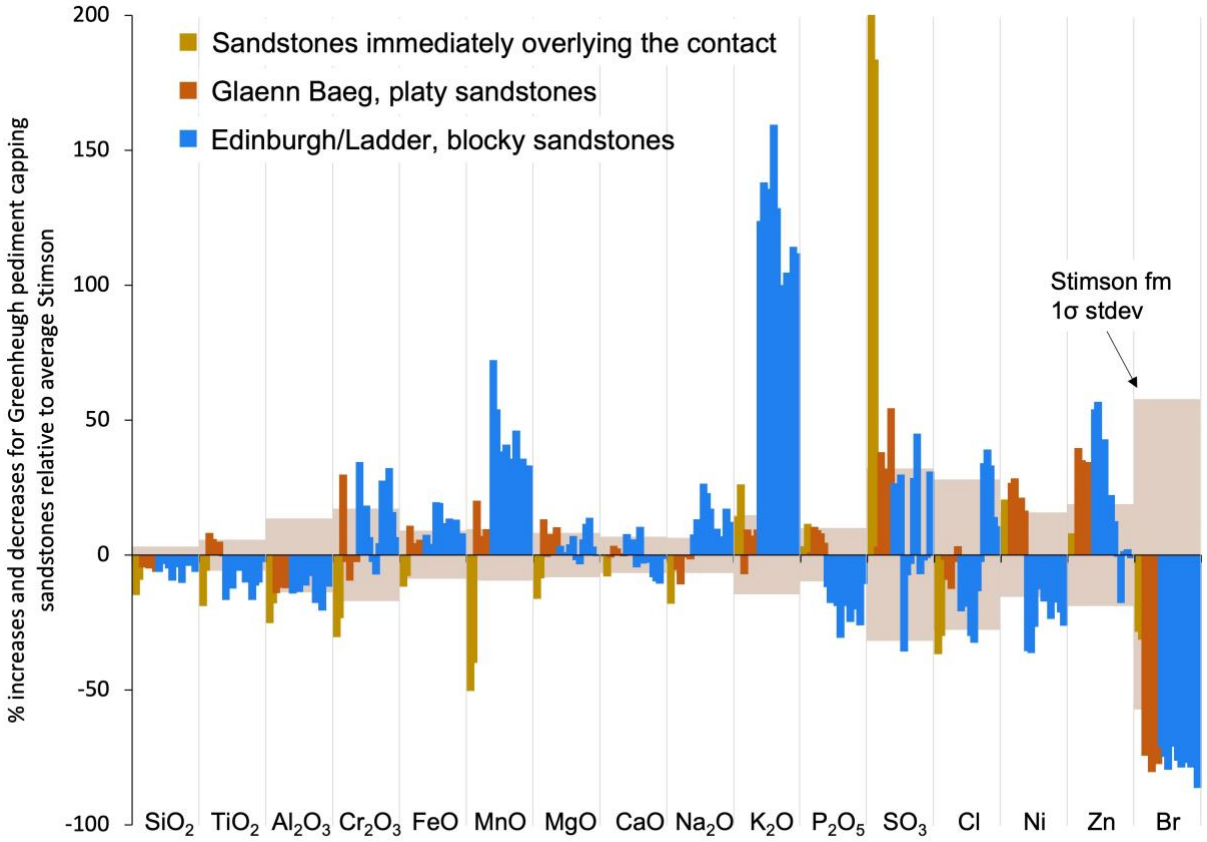

Figure 7. *Plot showing % elemental increases and decreases relative to average Emerson/Naukluft plateau, Stimson formation for; the Ladder and Edinburgh interval cap rock (blue), and the Gleann Beag interval cap rock (solid brown). The lighter brown denotes the two high S targets at the contact with the underlying Hutton interval. Shaded brown areas represent mimimum and maximum concentrations for the Stimson formation.*

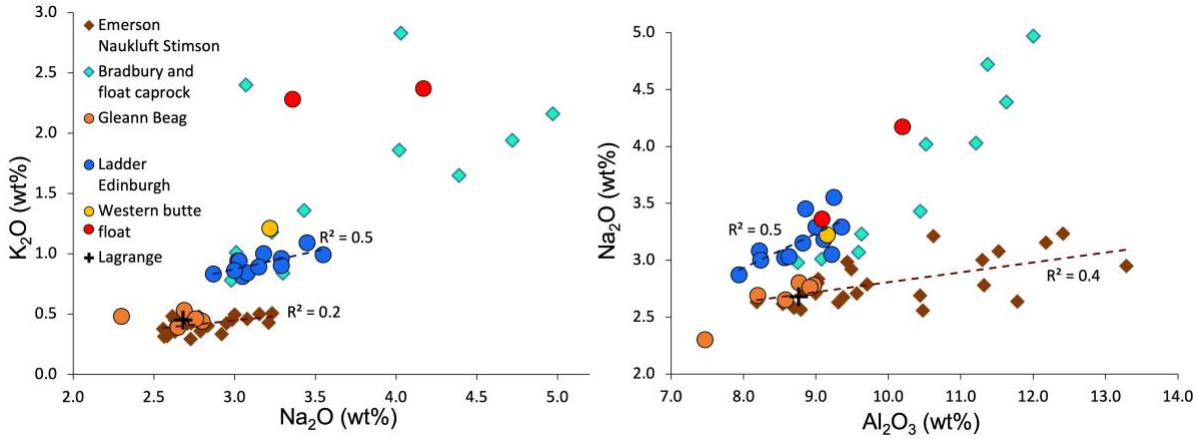

Figure 8*.Emerson/Naukluft plateau Stimson formation, Gleann Beag, Ladder and Edinburgh interval cap rocks, Western butte float cap rocks, and Bradbury rocks and float cap rock on K_2O versus Na_2O (left), and Na_2O versus Al_2O_3 (right) plots. In contrast to the Emerson/Naukluft plateau Stimson formation, the Ladder and Edinburgh interval cap rocks show moderate correlations of K and Na, and Na and Al.*

The Ladder and Edinburgh sandstones are also distinguished by moderate correlations between Na and K, and Na and Al (R^2 = 0.5 for both). This is in contrast to typical Stimson, which shows no correlation for Na and K (R^2 = 0.2), and only a very weak correlation between Na and Al (R^2 = 0.4) (Figure 8). The Gleann Beag sandstones plot with the Emerson and Naulkluft plateau Stimson targets.

3.2.4 Float cap rock from Western butte

Several loose blocks were analyzed on Western butte, the most likely origin for which is the morphologically and texturally similar cap rock exposure at the top of the butte (Figures 1d; S2, S9). The Blackwaterfoot target has the same elemental trends as the Ladder and Edinburgh interval sandstones from the pediment (Table 1b; Figure 6c, 8). The Lomond Hills and Heinrich Waenke rocks also have elevated K_2O (2.37 and 2.28 wt%), but concentrations are more than five times the K_2O of average Stimson (0.42 ± 0.08 wt%) (Figure 6d, 8). Lomond Hills and Heinrich Waenke have lower Cr_2O_3 (0.28 and 0.32 wt%), and trend to higher Na_2O (4.17 and 3.36 wt%), Ni (716 and 889 ppm) and Zn (1367 and 1876 ppm) concentrations than

424 Blackwaterfoot and the Ladder and Edinburgh interval sandstones on the pediment (274 – 522
425 ppm Zn; see 3.2.2. for Cr, Na, and Ni concentrations) (Figure 6d, 8).

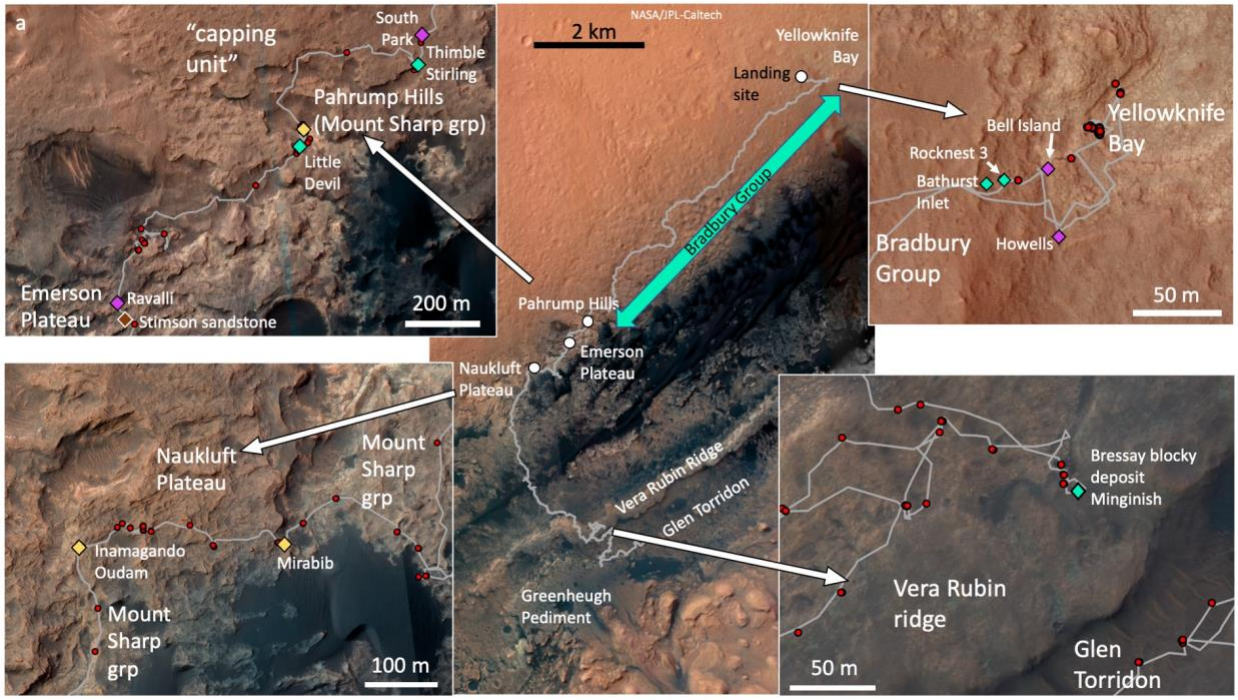

426

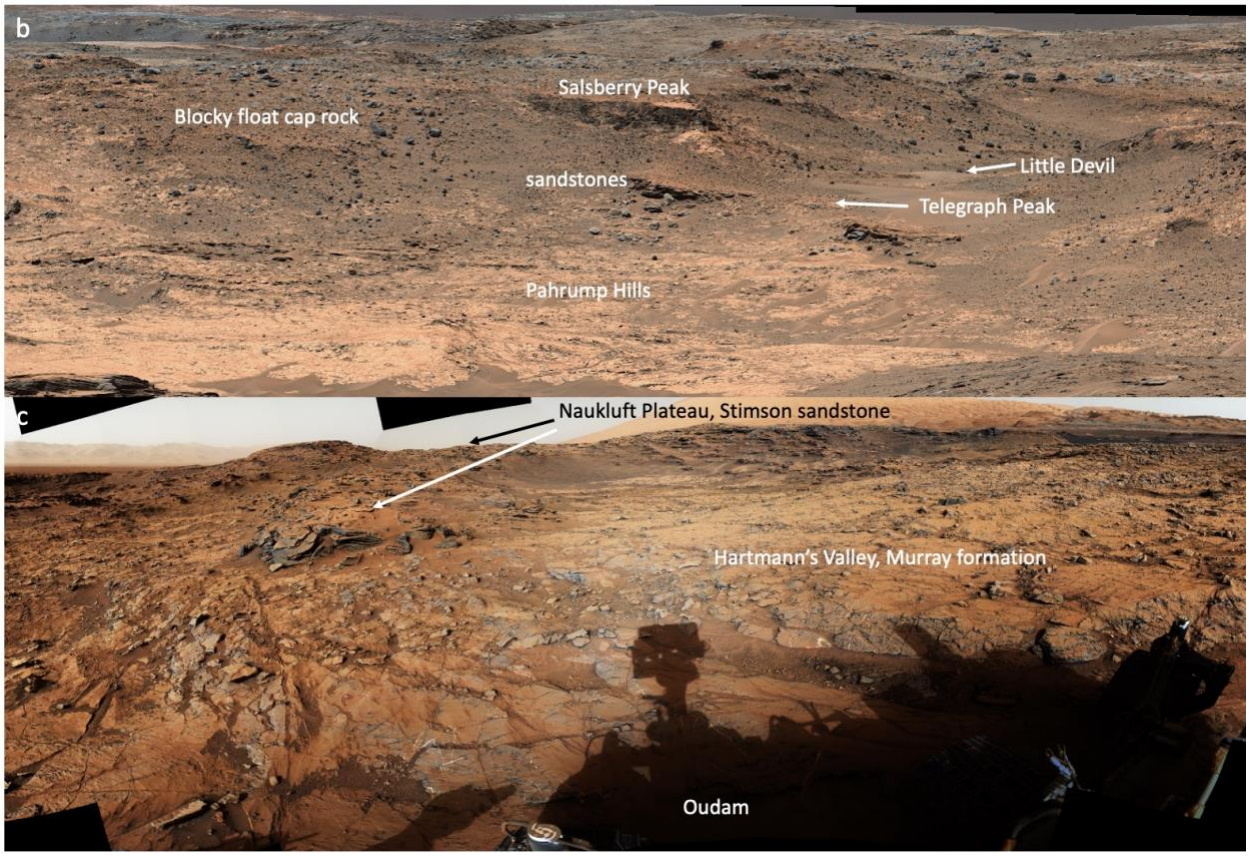

427

Figure 9. a) *Locations on HiRise imagery of previously encountered APXS targets that are compositionally related to pediment cap rock and the Hutton interval;* ***b)*** *Portion of Mastcam mosaic (mcam03214 - sol 747) showing the context of the Mount Sharp group at Pahrump Hills including the Telegraph Peak target and surrounding terrain, including Salsberry Peak capping sandstones and blocky float rocks, including the Little Devil float rock target;* ***c)*** *Portion of Mastcam mosaic (mcam06679 - sol 1367) showing the context of the Hartmann's Valley, Mount Sharp group just below the capping, Naukluft Plateau, Stimson sandstone at the Oudam drill site. Image credit for Mastcams: NASA/Caltech-JPL/MSSS*

3.2.5 Compositionally related targets to pediment cap rock

The blocky pediment capping sandstones and Western butte, Blackwaterfoot cap float block reveal related elemental trends to sandstone targets analyzed on Bradbury rise in the vicinity of Yellowknife Bay, as well as more resistant weathering, crater retaining cap rock encountered before *Curiosity* reached Pahrump Hills. Float cap rocks from the Mount Sharp group traverse, just below the Emerson plateau, also reveal comparable compositions (Figures 6e, 8, 9). Similarly, the Lomond Hills and Heinrich Waenke float cap rocks from Western butte exhibit elemental trends that are related to a number of sandstone, cap and float rock targets previously encountered on the mission; many of them also Bradbury group (Figure 6f, 8, 9).

4 Discussion and Implications

The APXS results from the investigation of the contact between the Mount Sharp group and Greenheugh pediment capping sandstones has revealed a number of compositional similarities to rocks encountered earlier in the mission. We discuss the significance and implications of these relationships.

4.1 Compositional similarity of the Hutton interval to other Mount Sharp group strata associated with the Basal Siccar Point group unconformity

The notably elevated Na, and excess Ca not associated with $CaSO_4$ within the Hutton interval immediately underlying the pediment, is also characteristic of several targets analyzed

454 by APXS at the base of the Mount Sharp group, within the Pahrump Hills and Hartmann's
455 Valley members. These include the bedrock targets: Topanga, Mescal, Puente, Pickhandle and
456 Telegraph Peak (Pahrump Hills member), and Mirabib, Inamagando and Oudam (Hartmann's
457 Valley member) (Table S1). More than 300 m of elevation and 3.5 km lateral distance separates
458 the Pahrump Hills and Hartmann's Valley targets from the Hutton interval at the pediment
459 contact (Figure 1). What is the relationship between these targets, if any, aside from a
460 compositional one?

461 The Pahrump Hills targets are also in proximity to capping sandstones and other blocky,
462 likely erosional remnants of alkaline cap rocks (Figure 9a, b). Specifically, the resistant Salsberry
463 Peak sandstones (represented by the APXS target, Little Devil) are exposed just above the
464 Telegraph Peak drill site (Figures 9a, b). The Mirabib, Hartmann's Valley target was the last
465 Mount Sharp group target analyzed by APXS before *Curiosity's* initial ascent onto the Naukluft
466 Plateau, Stimson formation sandstones, and Oudam and Inamagando are situated just below the
467 western extent of the plateau (Figures 9a, c). All the lower Mount Sharp group targets discussed
468 here are within 1 to 3m elevation of overlying capping sandstones (Salsberry Peak or Stimson).
469 Previous work has interpreted the Salsberry Peak sandstones to be a lens within the Mount Sharp
470 group (Kronyak et al., 2019; Stack et al., 2019) and therefore unrelated to the deposition of the
471 Stimson sandstones. Construction of a crosssection between the Salsberry Peak and Marias Pass
472 area (where *Curiosity* first encountered Stimson formation sandstones), reveals that the
473 sandstones are exposed at a similar elevation and could therefore be contemporaneous (Figure
474 10a), both overlying the Basal Siccar Point group unconformity.

475 Is the distinct chemistry relative to the rest of the Mount Sharp group preserved at these
476 widely dispersed, separate stratigraphic intervals related to changes in provenance and/or

sedimentological processes, or is it specifically related to the unconformity? If the compositional differences within the Hutton interval were the result of primary sedimentary processes, we would expect the zone to mimic the underlying, flat-lying stratigraphy (Stein et al., 2020). Instead, extrapolating the Hutton interval from Buchan Haven on Western butte to the Hutton drill site just below the pediment, reveals that it is dipping and cross-cuts the flat-lying stratigraphy. Furthermore, the dip of the Hutton interval mimics that of the unconformity, if extrapolated from the pediment to Western butte (Figure 10b). This indicates that at least at this location, the distinct chemistry is unlikely to be related to provenance or depositional processes, but is a result of proximity to the unconformity. Supporting this are the lack of obvious, sedimentological changes observed within the Hutton interval, relative to the rest of the Glasgow member. Furthermore, laterally equivalent Glasgow member targets analyzed by APXS after we drove east, away from the pediment, do not exhibit the same distinct chemistry as the Hutton interval, but instead reveal typical Glasgow member compositions (O'Connell-Cooper et al., this issue). They also exhibit the same spectral signatures as the rest of the Glen Torridon Mount Sharp group (Rudolf et al., this issue).

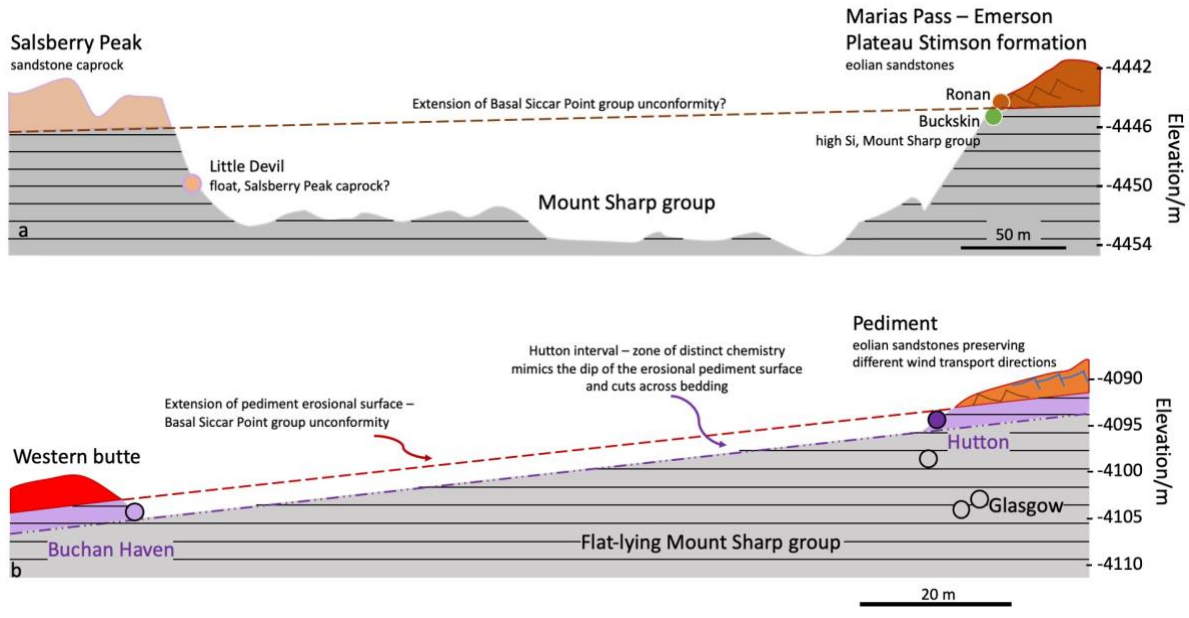

Figure 10: *Schematic cross-sections from* ***a)*** *Salsberry Peak (left) to Marias Pass (right). Note that the Stimson formation sandstones exposed at Marias Pass are at a similar elevation to Salsberry Peak capping sandstones and might also overly the Basal Siccar Point group unconformity (see Figures 9a & b for location of cross-section);* ***b)*** *Western butte (left) to where Curiosity ascended the pediment (right) (see Figure 2 for location of cross-section). Circles represent select APXS targets. Note how the compositionally distinct Hutton interval (purple) mimics the dip of the pediment erosional surface extended to the butte and cuts across the underlying flat-lying stratigraphy of the Mount Sharp group.*

The proximity of all the Mount Sharp group targets discussed above to the Basal Siccar Point group unconformity could be consistent with that erosional surface extending from the pediment, down to the lower Mount Sharp group at Pahrump Hills and Hartmann's Valley (Figure 11). Weathering along the exposed erosional surface prior to the deposition of the Siccar Point group could be responsible for the related chemistry. The distinct chemistry could also be the result of fluids interacting with the Mount Sharp bedrock immediately underlying the unconformity, both at the base of the Mount Sharp group and at the Hutton interval, after deposition and at least some lithification of the overlying sandstones.

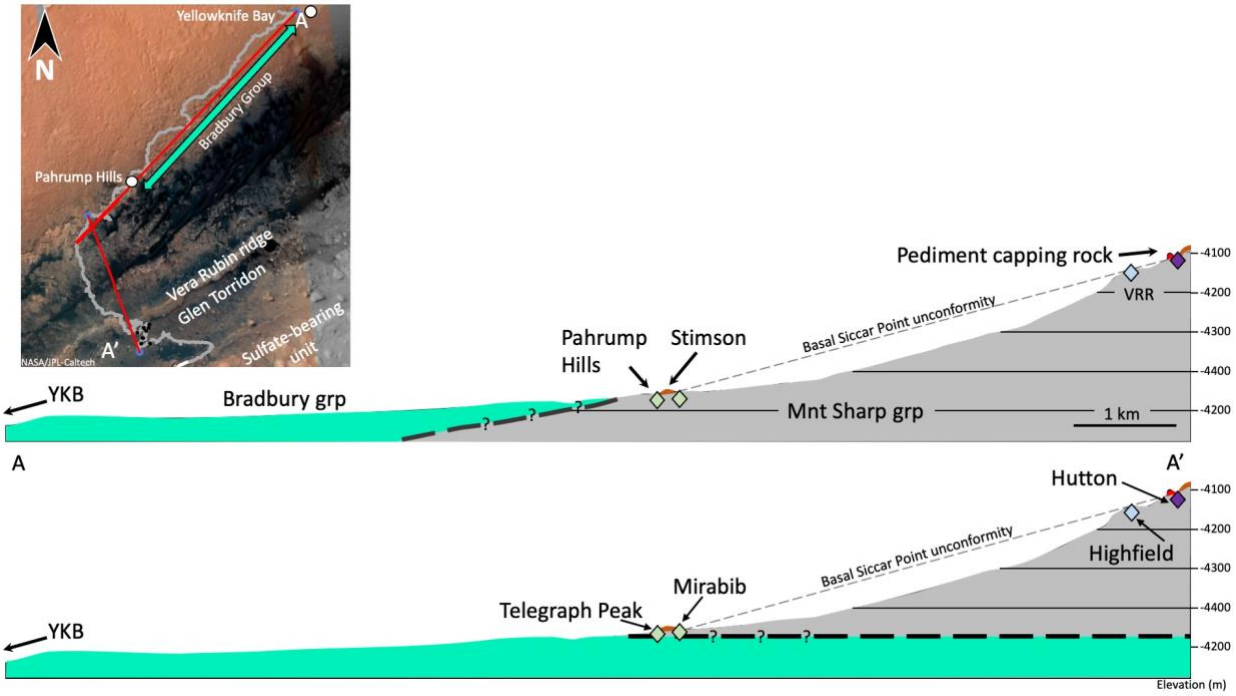

Figure 11. *Cross-sections drawn through A-A' shown on HiRise image top left; from the Yellowknife Bay area (left) to the pediment (right). Top cross-section depicts the scenario whereby both the Bradbury group and Stimson formation are younger than, and deposited onto the irregular erosional surface of the flat-lying Mount Sharp group. Bottom cross-section depicts the Bradbury group as older than the Mount Sharp group, with the Stimson formation being the youngest. Both show Basal Siccar Point group unconformity extrapolated from Pahrump Hills upto the pediment. Diamonds depict altered Mount Sharp group strata lying just below the unconformity.*

517
518 At least for the Hutton interval, these rocks would have undergone the same burial and
519 diagenesis as the rest of the Glasgow member, prior to erosion, and possible weathering and/or
520 alteration along the subsequent Basal Siccar Point group unconformity. Therefore, we can
521 compare the chemistry of the Hutton interval to the Glasgow DRT target to look for indicators of
522 one process over another. Weathering typically follows Cl>SO_4>Na>Ca>Mg>K>Si>Fe>Al>Ti
523 with respect to mobility of ions (decreasing mobility from left to right; Hudson 1995), This
524 results in concentration of the immobile elements, e.g., Ti, Al, Fe, Si, and depletion of the more
525 mobile ions e.g., Na, Ca, Mg, in the weathered horizon (e.g., Nesbitt & Wilson, 1992; Nesbitt &
526 Young, 1982). On Mars, weathering of the dominantly basaltic crust is expected to result in
527 liberation of Ca, Mg, Fe, S, and Cl, leaving residual Al, Fe, and Si (McLennan et al., 2003,
528 2019). However, compared to Glasgow, the Hutton interval targets show higher concentrations
529 of the mobile elements (Na, Ca, and Mg) and approximately the same or lower concentrations of
530 the immobile elements (Si, Al, and Ti) (Table 1a, Figures 3a, b). Furthermore, the mass balance
531 comparison of Hutton interval targets relative to Glasgow DRT indicates gains of the mobile
532 elements, Na, Ca, and Mg, as well as Fe and Mn, and the loss of S (Figure 4b). The lower
533 concentrations of Si, Al, and Ti are considered to be the result of addition of the mobile
534 elements. It therefore seems unlikely that chemical weathering has played a significant role in
535 the alteration of the Glasgow member rocks, and by inference, the similar composition Pahrump
536 Hills and Hartmann's Valley member rocks that would have been exposed along the erosional
537 surface.

538 4.1.1 Mineralogy and composition

539 The compositional relationships between the Hutton interval and lower Mount Sharp
540 group, Pahrump Hills targets are reflected in the mineralogy of the Hutton and Telegraph Peak

541 drilled samples, as determined by CheMin. The crystalline components of both samples are
542 dominated by plagioclase, pyroxene, magnetite>hematite, crystalline SiO_2 phases and potassium
543 feldspar (Rampe et al., 2017; Thorpe et al., this issue). Along with Buckskin (high SiO_2 Pahrump
544 Hills member drill sample), they are the only Mount Sharp group drill samples with magnetite as
545 the dominant Fe-oxide phase detected. Both have minor fluorapatite and minor to absent
546 crystalline $CaSO_4$ phases, consistent with the P, Ca, and S measured by APXS.
547 The Hutton and Telegraph Peak samples, along with Oudam, Buckskin and Highfield
548 (grey/blue Jura member drill sample from Vera Rubin ridge), have the lowest clay mineral
549 abundances detected of the Mount Sharp group drill samples (<6 wt %) (Rampe et al., 2020b;
550 Thorpe et al., this issue). The Buckskin drill hole is located only 0.2 m from the contact with the
551 unconformably overlying Stimson formation sandstone and the Highfield drill site is interpreted
552 to have been situated just below the extrapolation of the pediment capping sandstone over the
553 Vera Rubin ridge (Figure 11) (Bryk et al., 2019; Fraeman et al., 2020).
554 Opal-CT is also detected in all the low clay abundance Mount Sharp group drill samples
555 (4-11 wt %) and not in any other Mount Sharp group drill sample (Rampe et al., 2020b). In
556 contrast to Hutton, the Glasgow drill sample, situated ~6 m below the pediment, has 23.5 wt%
557 clay mineral abundance, hematite>magnetite, calcium sulphates, only ~1 wt% crystalline SiO_2,
558 and no opal-CT; the same as other Glen Torridon drill samples (Thorpe et al., this issue).
559 The plagioclase abundances are also distinct for Hutton versus Glasgow (26.5 versus 15.4
560 wt% respectively), as are their derived compositions (An_{25} and An_{47}, respectively; Thorpe et al.,
561 this issue). The more sodic plagioclase composition of the Hutton drill sample is consistent with
562 the elevated Na measured by APXS. Therefore, most of the excess Ca (which is not associated
563 with $CaSO_4$ phases) in the Hutton sample cannot be attributed to differences in plagioclase

content (i.e., higher calcic plagioclase abundance in Hutton). Instead it is probably related to the higher pyroxene abundance in the Hutton sample, the detection of fluorapatite and the greater CaO content of the amorphous component of Hutton versus Glasgow. Telegraph Peak also has a more sodic plagioclase component compared to the other Pahrump Hills drill samples (Rampe et al., 2017), consistent with the elevated Na measured by APXS in that sample and related targets (Thompson et al. 2020).

4.1.2 Implications

The proximity of the Hutton interval and other geochemically and mineralogically related Mount Sharp group targets to the Basal Siccar Point group unconformity suggest that the contact provided a conduit for enhanced fluid flow. The absence of appreciable $CaSO_4$ and low clay content are consistent with an alteration event associated with the unconformity that resulted in the dissolution of those phases after deposition of the cap rock and post-dating the process that concentrated clay and $CaSO_4$ minerals throughout the rest of the Mount Sharp group (e.g., Achilles et al., 2020; Bedford et al., 2019; Bristow et al., 2018, 2021; Hurrowitz et al., 2017; Rampe et a;l 2017, 2020b; Thorpe et al., this issue). Based on the chemistry, the silica phases detected by CheMin in the Hutton drill sample are not the result of the addition of silica, but must instead be the result of the dissolution of pre-existing silicates, which could include clay minerals. The fluid responsible for the alteration would have been concentrated in the mobile cations Na, Ca ,and Mg and to a lesser extent Fe and Mn.

The presence of opal-CT and coarse grained, grey hematite in the Highfield and Oudam drilled samples has been proposed by Achilles et al. (2020) and Rampe et al. (2020a) to be the result of alteration by relatively warm (~100°C) diagenetic fluids. While grey hematite has not been detected by CheMin within the Hutton drilled sample, Rudolf et al. (this issue) observe

spectral signatures within Hutton interval strata consistent with grey hematite. Therefore, we suggest that the related chemistry and mineralogy observed within the Hutton interval is the result of interaction with similar diagenetic fluids. The occurrence of magnetite, cristobalite, opal-CT, sodic feldspar compositions and the lack of $CaSO_4$ are consistent with alteration by relatively warm, near neutral pH, possibly briney fluids. For example, Bonyadia & Sadeghib (2020) describe sodic and calcic alteration associated with the formation of hydrothermal iron oxide deposits in the Bafq iron deposits, Iran. Minerals formed during the alteration include sodic plagioclase, magnetite and apatite. They invoke the hydrothermal heating of brines, derived from evaporite basins and the action of fluids with high Na/K and Cl/S ratios. The action of a briney fluid would also be consistent with lack of $CaSO_4$ detected by either APXS or CheMin. Brines enhance the solubility of $CaSO_4$ (Klimchouck, 1996).

The Moorfoot Hills diagenetic target indicates addition of $CaSO_4$ to a Hutton-like bedrock with pre-existing excess CaO. This is consistent with the $CaSO_4$ addition occurring after the event that resulted in the excess CaO in the Hutton interval bedrock. The association of the Moorfoot Hills, Liberton Brae, Dunbartonshire and Dounraey targets with the same vein that cross-cuts the Hutton workspace, and the compositionally related, cross-cutting Abernethy vein target in the Buchan Haven workspace, is further evidence for the late-stage timing. If the vein system was emplaced prior to the CaO enrichment of Hutton interval bedrock, we might expect all the analyses to plot with excess Ca, which they do not. The distinct and varied chemistries of the different diagenetic features within the Hutton workspace suggest complicated and multistage fluid interactions associated with their formation, necessarily including the mobility of Fe, Mn, Mg, and K.

609 Similar veins and diagenetic features to those within the Hutton drill workspace were not
610 observed within the overlying pediment-capping sandstones. This might indicate that the vein
611 system was emplaced prior to the deposition and lithification of the sandstones, contradicting the
612 above argument. However, *Curiosity* has only examined a relatively small area of the overlying
613 pediment-capping sandstones, so the presence of similar features cannot be discounted. They
614 may also be more difficult to identify within the darker grey, more resistant pediment-capping
615 sandstones. The sandstones may also have had a different response to the stresses that formed the
616 veins in the underying Hutton interval.

617 4.2 Compositional relationship of Greenheugh pediment cap rock to Stimson formation

618 4.2.1 Gleann Beag interval sandstones

619 The platier pediment sandstones exposed at the base of the section (Gleann Beag interval,
620 Banham et al., this issue) are compositionally in family with previously analyzed Stimson
621 formation sandstones. Therefore, they were probably deposited in a similar environment, with a
622 related provenance; i.e., aeolian, not dissimilar to Bagnold sand with a basaltic source
623 (O'Connell-Cooper et al., 2017). The Gleann Beag interval is interpreted to represent the
624 remnants of oblique compound dunes, with the same wind transport direction (to the northeast)
625 as the those preserved at Murray buttes (Banham et al., this issue). Whether the sandstones
626 exposed within the Gleann Beag section on the pediment are contemporaneous with those
627 observed at Murray buttes cannot be determined from the available data; however, it can also not
628 be ruled out. The statistically distinct Si, Al, P, Ni, and Zn concentrations of the pediment
629 capping Gleann Beag sandstones from typical Stimson sandstones might indicate that they were
630 not deposited at the same time, perhaps under somewhat different depositional regimes (Banham
631 et al. 2018 and 2021). However, the Si, Al, P, Ni, and Zn concentrations of the two overlap and a

minor change in the sediment input and/or slightly contrasting post-depositional diagenesis of the sandstones could also account for the compositional differences.

4.2.1.1. Diagenesis/alteration of the Gleann Beag sandstones

The nodular sandstone targets analyzed within the Gleann Beag section have related compositions to the less nodular Galloway Hills target, as well as Naukluft and Emerson Plateau Stimson sandstones. This indicates that their formation was associated with essentially isochemical processes. In contrast, high S detected in the two targets analyzed immediately at the contact with the underlying Mount Sharp group indicates interaction with S-rich fluids, focused along the contact. The mass balance calculation relative to the Galloway Hills target indicates addition of significant S, some K and P, and the possible loss of Mn and Cr (Figure 12a). Hence the additional S is not associated with $CaSO_4$ (Figure 12 b). Investigation of the more nodular targets via the same mass balance calculation suggests the same relationships, but far less pronounced. This might indicate that the same fluids were responsible for the formation of the nodules, but that the fluid became rapidly diluted away from the contact.

The underlying Hutton interval targets all exhibit low sulfur concentrations relative to the rest of the Glasgow member, other Glen Torridon rocks, and most of the Mount Sharp group (§3.1, Figures 3, 12b). Sulfur may have been mobilized during alteration of the Hutton interval strata along the Basal Siccar Point group unconformity and precipitated in the sandstones immediately overlying the contact, perhaps in response to a change in porosity/permeability. If this is the case, it supports alteration of the underlying Mount Sharp group after deposition of the overlying sandstone. It also provides some constraints on the source of fluids responsible for the alteration of the underlying Hutton interval. They are unlikely to have passed through the pediment capping sandstones prior to interaction with the Hutton interval, and instead were

655 probably focused just beneath the contact, along the unconformity, with only limited migration
656 into the overlying sandstones.
657

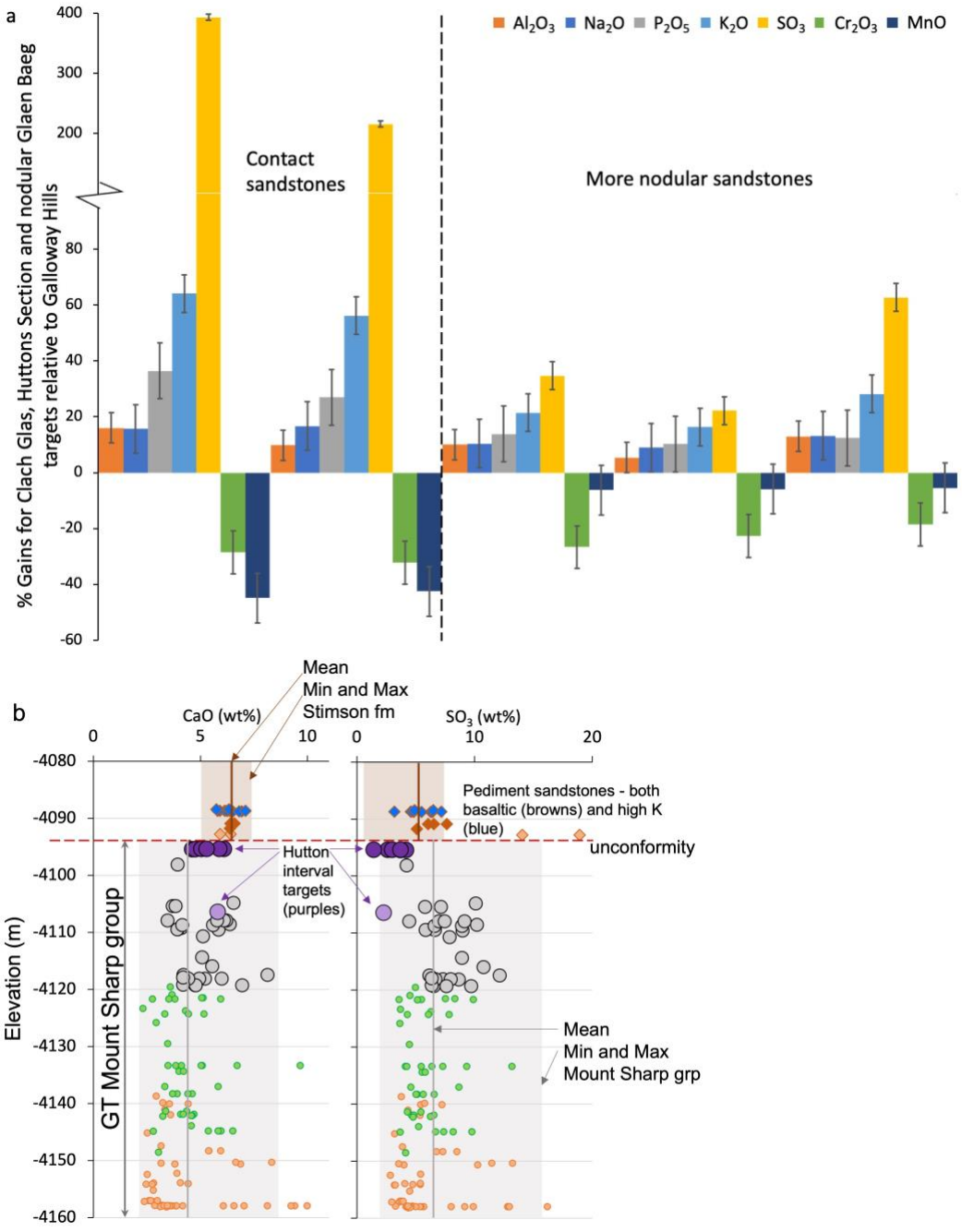

658
659
660 ***Figure 12. a)*** *Plot representing the results of a mass balance calculation for the high S and nodular sandstones*
661 *relative to Galloway Hills (Table S4 and §S2.8.). Note change of scale above 100%;* ***b)*** *Plots of CaO and SO_3*
662 *concentrations versus elevation for the GT Mount Sharp group and pediment capping sandstones. Note the very low*

S associated with the Hutton interval targets and the elevated S in the two pediment sandstones immediately above the Basal Siccar Point group unconformity.

4.2.2. Ladder and Edinburgh interval sandstones

The blocky pediment sandstones (Ladder and Edinburgh intervals; Banham et al., this issue) are compositionally distinct from the platier (Gleann Beag) sandstones and the Stimson formation sandstones encountered earlier in the mission. The different chemistry of these sandstones is consistent with their contrasting sedimentology (Banham et al., this issue). The sandstones exposed within the Ladder interval (APXS targets: Forsinard Flows and Machir Bay) represent straight-crested simple dunes, with a southerly wind transport direction. The Edinburgh interval sandstones (APXS targets: Glen Feshie, Assynt Window, Edinburgh, and Eshaness) are trough cross-bedded and were deposited in a westerly wind transport direction. These transport directions are in contrast with the north-northeast directions preserved within the basal Gleann Beag interval sandstones and the Stimson formation sandstones exposed on the Naukluft and Emerson plateaus and at Murray buttes (Banham et al., 2018, 2021). There are indications, based on analysis of MAHLI images (Figure S14), that the higher K sandstones are also generally coarser grained, and preserve somewhat more rounded grains than the basal Gleann Beag sandstones (Banham et al., this issue). Therefore, the compositional differences between the lower and upper pediment sandstones are most likely reflecting changes in provenance and/or depositional environment.

4.2.2.1 Mineralogy and composition

The higher potassium feldspar abundance of the Edinburgh drill sample (3.4 wt%; Thorpe et al., this issue) compared to the Stimson formation Big Sky (1.1 wt%) and Okoruso (1.9 wt%) drill samples from the Naukluft plateau (Yen et al., 2017) is consistent with the elevated K measured by APXS. The detection of olivine (8.3 wt%) and smectite (7 wt%) (Thorpe et al., this

688 issue), phases not found above detection limits in the Big Sky and Okoruso samples (Yen et al.,
689 2017), might explain the higher Fe, Mn and Cr measured by APXS if the olivine and/or smectite
690 were relatively Fe-rich. SAM EGA and CheMin data indicate that the Edinburgh phyllosilicate is
691 an Fe-rich dioctahedral smectite (Sutter et al., 2020; Rampe et al., 2020c). These differences in
692 mineralogy (and chemistry) between the Naukluft Plateau Stimson formation and the Edinburgh
693 pediment capping sandstone could be consistent with changes in provenance between the two.
694 The coarser grain size of the high-K sandstones (Banham et al., this issue) indicates that
695 transport/sorting processes may also be responsible for at least some of the differences in
696 chemistry. The detection of olivine could be consistent with the coarser grain size measured.
697 Olivine is more resistant to mechanical breakdown than softer minerals and those with cleavage;
698 it would therefore be expected to reside in the coarser eolian size fraction, as has been observed
699 for the active Bagnold sands (O'Connell-Cooper at al., 2017). If potassium feldspar formed
700 relatively large crystals in an igneous source rock compared to plagioclase, this could also
701 explain the concentration of potassium feldspar in coarser sand fractions, and the higher K
702 concentrations measured by APXS. A coarser grain size might also indicate a more proximal
703 source, although all pediment sandstones show rounded grains, which would suggest no
704 significant change in transport distance. However, the Ladder and Edinburgh sandstones are
705 described as exhibiting somewhat more rounding of grains than the basal Gleann Beag
706 sandstones (Banham et al., this issue). This could be consistent with reworking of already
707 rounded grains from a more proximal, pre-existing sedimentary rock.
708 Big Sky, Okoruso and Edinburgh all have potassium feldspar (1-3 wt%); neither the
709 inactive Rocknest soil, nor the two active sand samples contain potassium feldspar above the
710 detection limits of CheMin (Achilles et al., 2017; Rampe et al., 2018). All but three of the

711 mudstone samples analyzed by Chemin have potassium feldspar (3-9 wt%; Rampe et al., 2020b),
712 and the Windjana sandstone comprises 26 wt% potassium feldspar (Treiman et al., 2016). Could
713 the potassium feldspar detected in the ancient eolian deposits be derived from local erosion of
714 pre-existing Gale crater mudstones, such as the Murray formation, or more likely, high-K
715 sandstones (e.g., Windjana), and mixing of this material with more basaltic source rocks? In this
716 scenario, the higher-K pediment sandstones contain more of this locally derived detritus than the
717 rest of the Stimson formation. The Windjana sandstone also contains 10% smectite (Treimann et
718 al., 2016) and the majority of the Mount Sharp group drilled samples contain significant clay
719 mineral abundances (Thorpe et al., this issue). Thus, at least the phyllosilicate detected within
720 the Edinburgh sample might reflect a more proximal input. The difference in composition and
721 mineralogy might also reflect input from different composition igneous source rocks relative to
722 the rest of the Stimson formation and Gale soil and sand (e.g., Schmidt et al., 2014; Treiman et
723 al., 2016; Thompson et al., 2016). See §4.3 for further discussion.

724 Given the correlation of the chemistry with detrital mineralogy, weathering is unlikely to
725 have played a significant role in the differences observed. Potassium feldspar is more resistant to
726 weathering than plagioclase (Goldich, 1938). Its detection could therefore indicate increased
727 weathering either at source or post-depositionally for the Ladder and Edinburgh interval
728 sandstones relative to the rest of the Stimson. However, the olivine detection in the Edinburgh
729 drill sample is not consistent with this; the preservation of olivine indicates only minimal
730 weathering and aqueous alteration.

731 Hausrath et al. (2018) attribute the lack of olivine, and greater magnetite content of the
732 drilled Big Sky and Okoruso Stimson samples versus the eolian Rocknest and Gobabeb samples
733 to diagenesis by near-neutral pH aqueous solutions. They propose the dissolution of olivine and

precipitation of magnetite by solutions enriched in sulfate and chloride. They do not consider weathering/alteration of the source material prior to erosion, differences in igneous mineralogy at the source, sorting/transport processes, nor the fact that magnetite could be detrital. Applying their model to the Edinburgh drill sample is not consistent with both the high magnetite and olivine content detected by CheMin, unless there was significantly more olivine in the sand prior to diagenesis.

4.3 Compositional relationship of the high-K pediment capping rocks to other Gale crater lithologies

The Ladder and Edinburgh interval sandstones, and Blackwaterfoot float from Western butte reveal elemental trends related to a number of Bradbury group sandstones and float cap rock targets analyzed along the Mount Sharp group traverse (Figures 6c, 8). These including Bell Island (sandstone exposed just above Yellowknife Bay) and Howells and Eqaluik (Shaler fluvial sandstone, also just above Yellowknife Bay – Bradbury group), South Park (example of Bradbury group, capping unit sandstone analyzed just before Pahrump Hills), and the Ravalli float cap rock analyzed as we traversed the Hartmann's Valley member adjacent to the Emerson Plateau (Table S1; Figures S17, S20, S24).

The Lomond Hills and Heinrich Waenke cap float rock targets analyzed on Western butte are also compositionally related to other Bradbury group sandstones and cap rock targets (Figures 6d, 8). These include Minginish (float rock on VRR), Little Devil (interpreted to represent the Salsberry Peak cap sandstone at Pahrump Hills), Stirling and Thimble (capping unit sandstone analyzed nearby South Park, prior to Pahrump Hills), Bathurst and Rocknest 3 (Bradbury group sandstones just above Yellowknife Bay), and Ravalli (see above) (Table S1; Figures S18, S19, S21, S22, S24).

The locations of these compositionally related targets previously encountered by *Curiosity* are shown on Figure 9. Note that a number of them are in the vicinity of one another, and that all the cap rock float targets on the Mount Sharp group traverse (except Minginish) are in proximity to either the Emerson or Naukluft plateaus or Murray buttes Stimson formation. Minginish is a small boulder within the Bressay blocky deposit on VRR, which also included a sandstone target, Rousay (sol 2019), with a typical Stimson composition. Many of these rocks are also texturally alike, appearing relatively smooth, resistant to weathering, and blockier in appearance than typical Stimson sandstone and the platier sandstones exposed at the base of the pediment capping unit (see images in §S3 and S4).

4.3.1 Implications

The comparable compositions and textures of the high-K pediment cap rocks and the Western butte float rocks to Bradbury group rocks and float, indicate that they are related to one another. The proximity of the Bradbury-like float rocks to Stimson formation sandstones and the occurrence of both typical Stimson and high-K composition sandstones on the pediment also point to a relationship.

The Bradbury group sandstones analyzed just above Yellowknife Bay are separated by more than 9 km laterally and ~400 m in elevation, from the pediment capping sandstones. The large lateral separation is most easily explained by shared provenance and/or depositional processes for the sandstones versus the same style of post-depositional alteration. This is supported by the relationship between the composition and detrital mineralogy of the Edinburgh samples. The Bradbury group is interpreted to have been derived from the mixing of multiple, diverse igneous source rocks including basaltic and more alkaline and silica rich lithologies (Bedford et al., 2019; Cousin et al., 2017; Edwards et al., 2017; Sautter et al., 2015; Schmidt et

al., 2014; Stolper et al., 2013; Thompson et al., 2016; Treiman et al., 2016). We therefore propose that the Ladder and Edinburgh interval sandstones, as well as the float rocks analyzed on Western butte, are derived from similar source rocks to the Bradbury group sandstones.

The current stratigraphic column depicts the Bradbury group as being older than the Mount Sharp group. However, given the argument above, could the Bradbury group and the Stimson formation both be younger than the Mount Sharp group and related (Figure 11)? The Mount Sharp group might represent relatively old lacustrine/fluvial deposits, which were buried, lithified and then eroded, before deposition of the Bradbury and Siccar Point groups onto that erosional surface, thus explaining the differences in elevation between the two groups. This is not the first time such a scenario has been proposed. Wiens et al. (2020) suggest that at least parts of the Bradbury group, i.e., the layered rocks at Bathurst Inlet, and other similar composition, layered float rocks from the Bimbe heterolithic deposit (another blocky deposit on the Mount Sharp Group), have the same provenance and were deposited at the same time. In their model, both are younger than, and would have overlain, the Stimson formation and along with it, draped over the underlying erosional topography.

An alternative is that there is at least one, more alkaline (than an average martian basaltic) source area in and around Gale crater that has been eroded by both water and wind at different times during the history of the evolution of the crater and its infill. The Bradbury group alkaline sedimentary rocks would have been deposited prior to the more basaltic Mount Sharp group, followed by the basaltic and alkaline Siccar Point group eolian rocks (Figure 11). Both scenarios are consistent with widespread evidence at Gale crater for the presence of multiple igneous source rocks.

4.3.2 Relationship to Gediz Vallis ridge

803 The Gediz Vallis ridge, south of the pediment (Figure 2) appears to contain
804 abundant large, dark blocks and boulders. (Bryk et al., 2019; Hughes et al., 2019). Could the
805 Gediz Vallis ridge be the source of the high-K and -Na Lomond Hills/Heinrich Waenke float cap
806 rocks and the material that capped Western butte? If so, what is the relationship between the
807 boulders within the Gediz Vallis ridge, cap rocks and Bradbury group targets previously
808 encountered on the mission? Bryk et al. (2019) have proposed that the Gediz Vallis ridge deposit
809 could once have extended to VRR and may be the source of the Bressay boulder deposit
810 containing the high-K, Minginish, and Stimson-like composition, Rousay float blocks. The
811 Bradbury group has generally been interpreted to have been sourced from the Gale crater rim or
812 beyond (Palucis et al., 2014), whereas the material that comprises the Gediz Vallis ridge is
813 thought to have been sourced from higher up on Mount Sharp (Bryk et al., 2019), which does not
814 seem to fit with them being genetically related. If the Western butte cap float rocks did originate
815 in Gediz Vallis, the valley could be sourcing material/boulders from some overlying strata that
816 was once more extensive and related to Bradbury group rocks.

817 4.3.3 The role of diagenesis

818 Another scenario is that the blockier, high-K, pediment-capping sandstones underwent
819 more diagenesis/cementation than the platier, low-K pediment sandstones, and that this is the
820 source of the distinct chemistry. This would be consistent with their blockier and smoother
821 appearance and would imply that a K- (and Mn-, Na-) rich fluid may have been involved.
822 The Edinburgh drill sample contains phyllosilicate, which was not detected in previous Stimson
823 drill samples (Rampe et al., 2018; Thorpe et al., this issue). If the phyllosilicate is authigenic, it
824 implies a different post-depositional diagenetic/alteration history for the blocky pediment

825 sandstones versus the Stimson formation at the Naukluft and Emerson plateaus. However, given
826 the arguments in §4.2.2.1. the phyllosilicate is most likely reflecting a local detrital input.
827 Coarser sandstones would be expected to have had higher initial porosity and
828 permeability than finer grained sandstones at the time of deposition, and might therefore undergo
829 more diagenesis. Therefore, the coarser Ladder and Edinburgh section sandstones might be
830 expected to be better cemented than the finer grained Gleann Beag sandstones. Given the
831 sedimentological differences between the Gleann Beag, and Ladder and Edinburgh interval
832 sandstones, the correlation of the chemistry with the detrital mineralogy, and the relationship to
833 rocks encountered much earlier in the mission, this is not the most plausible explanation.
834 However, even if provenance and sedimentary processes are primarily responsible for the
835 difference in chemistry of the capping sandstones versus the Emerson and Naukluft Plateau
836 Stimson sandstones, the distinct detrital mineralogy might have driven different post-
837 depositional diagenetic reactions.
838 4.4 Proposed series of events
839 The following proposed series of events are based on the compositional, mineralogical
840 and sedimentological data. The Mount group strata was deposited in a predominantly lacustrine
841 environment followed by burial and diagenesis/alteration to give the clay rich, $CaSO_4$ – bearing,
842 relatively homogeneous in composition, Mount Sharp group. This was followed by erosion of
843 the Mount Sharp group, and later deposition of the eolian sandstones (Siccar Point group,
844 Stimson formation) onto that erosional surface. The Bradbury group sandstones may also have
845 been deposited at this time. The Stimson sandstones had both basaltic and more alkaline
846 composition source regions and probably incorporated some more proximal sediment as
847 evidenced by the clay mineral detection in the Edinburgh drill sample. The sandstones were then

848 subject to at least some burial and diagenesis, prior to fluid flow focused along the Basal Siccar
849 Point group unconformity. This resulted in the alteration of the underlying Mount Sharp group
850 within ~3 m and over at least 4 km laterally along the contact, and destruction of both clay and
851 calcium sulfate minerals. The localized dark veins and associated diagenetic features within the
852 Hutton interval (e.g. Dounraey-Dumbartonshire), and crosscutting $CaSO_4$ veins were the last to
853 form, with distinct fluid chemistries from those responsible for the alteration of the Hutton
854 interval strata.

855 **5 Conclusions**

856 *Curiosity's* investigation of the Greenheugh pediment capping rocks and immediately
857 underlying strata, and the compositional data acquired by APXS have revealed relationships with
858 a number of lithologies examined earlier in the mission. These relationships provide important
859 insights into regional and crater-scale processes within Gale crater and evidence for the long-
860 lived role of water and aqueous alteration and hence, habitable environments.

861 The Stimson formation strata encountered on the pediment preserves a record of eolian
862 transport and deposition of both more basaltic and alkaline detritus; the basaltic sand being
863 sourced from the south, and the more alkaline sand from the north. The relationship of the
864 alkaline composition, pediment-capping Stimson formation to Bradbury group sandstones and
865 cap rock lends further credence to the presence of alkaline igneous source rocks within, and in
866 the vicinity of Gale crater, concentrated to the north of *Curiosity's* location. This source rock
867 would have provided the sediment input to both fluvial and eolian sandstones, which may have
868 been deposited more or less contemporaneously. In this scenario, the Bradbury group and Siccar
869 Point group are both younger than the Mount Sharp group. Alternatively, erosion and transport
870 of alkaline source rock by both wind and water may have occurred at different times during the

evolution of Gale crater, separated by millions of years, i.e., the Bradbury group is older than both the Mount Sharp and Siccar Point groups.

Identification of compositionally and mineralogically distinct Mount Sharp group strata only exposed within 3 m elevation of the Basal Siccar Point group unconformity, both at the base of, and more than 300 m higher up the section, indicates a relationship to that unconformity. We suggest fluid flow focused along the contact between the Mount Sharp group rocks and the overlying, relatively impermeable Siccar Point group sandstones, altered Mount Sharp group strata within 3 m of the contact. This alteration resulted in the loss of S and addition of Ca, Mg and Na to typical Mount Sharp group strata, manifest by the loss of clay minerals and calcium sulfate and the formation of magnetite, opal-CT and cristobalite, and more sodic plagioclase. The fluid had limited interaction with immediately overlying sandstones, resulting in the addition of S to strata within 10s of cms of the contact. Cross-cutting dark-toned veins and associated features provide evidence for complicated, late stage alteration, with multiple distinct chemistries.

Curiosity will soon transition onto the Greenheugh pediment again, at a lateral distance of ~1 km and an elevation gain of ~100 m from the original ascent. Will there be any relationship to the compositional changes we observed within the Hutton interval and those detected lower down in the Mount Sharp group stratigraphic section along the Basal Siccar Point unconformity? Will we see the same stratigraphy, sedimentology and chemistry within the pediment capping rocks as observed on our initial ascent of the Greenheugh pediment? *Curiosity* might discover in situ high-K and -Na rocks equivalent to the Western butte float rocks. *Curiosity* will also investigate the edge of the Gediz Vallis deposit. There could be a compositional relationship

between the Gediz Vallis deposit and the high-K float cap rocks encountered on Western Butte, and other heterolithic blocky deposits?

Acknowledgments

MSL APXS is managed and financed by the Canadian Space Agency (CSA). We acknowledge the important role of the engineers at JPL, the MSL science team and everyone involved in operations with respect to obtaining APXS data. Mastcam mosaics were processed by the Mastcam team, and MAHLI images and mosaics were processed by the MAHLI team at Malin Space Science Systems.
Science team member funding for Thompson, Boyd, Gellert, O'Connell-Cooper, and Spray is provided by the CSA. Yen acknowledges that a portion of this research was carried out at the Jet Propulsion Laboratory, California Institute of Technology, under a contract with the National Aeronautics and Space Administration. Berger was funded by a NASA Postdoctoral Program fellowship administered by USRA. VanBommel was supported by NASA/Caltech/JPL Contract 1549716 to Washington University in St. Louis for participation in the Mars Science Laboratory Science Team.

Data Availability

All MSL, raw data are available at the planetary data system:
https://pds-geosciences.wustl.edu/missions/msl/index.htm
https://an.rsl.wustl.edu/msl/mslbrowser/an3.aspx
All raw APXS data used in this study is available at the planetary data system: https://pds-geosciences.wustl.edu/msl/msl-m-apxs-4_5-rdr-v1/mslapx_1xxx/data/ and http://doi.org/10.17189/1519440
All APXS Murray formation data upto and including VRR presented in this paper is available at: *Thompson, L. (2020). Alpha Particle X-ray spectrometer geochemistry of the Murray formation and Vera Rubin ridge, Gale crater, Mars. https://doi.org/10.25545/ZXDJZ7, UNB, V1, UNF:6:bL/a2qTZBu6DNJlzkmGAbg==[fileUNF]*

All tables within the manuscript and supporting information, as well as derived data can be found at: *Thompson, L. (2022). Alpha Particle X-ray spectrometer geochemistry of rocks associated with the Basal Siccar Point group unconformity, Glen Torridon region, Gale crater, Mars.* doi to be supplied upon final submission. For review purposes, Excel files have been uploaded as supplementary files. Names correspond with relevant figures.

Other manuscripts submitted to this special issue referenced herein:

Banham et al., (this volume), Evidence for seasonal- to millennial-scale wind fluctuations in an ancient aeolian dune field: Reconstruction of the Hesperian Stimson formation at the Greenheugh pediment, Gale crater, Mars

Bennett et al., (this volume), An Overview of the Curiosity rover's Campaign in Glen Torridon, Gale Crater, Mars. Journal of Geophysical Research: Planets.

Caravacal et al., (this volume), From lake to river: Documenting an environmental transition across the Jura/Knockfarril Hill members boundary in the Glen Torridon region of Gale crater (mars).

Gasda et al., (this volume),

O'Connell-Cooper et al., (this volume), Statistical analysis of APXS-derived chemistry of the clay-bearing Glen Torridon region and Mount Sharp group, Gale crater, Mars

Rudolf, et al., (this volume), The distribution of clay minerals and their impact on diagenesis in Glen Torridon, Gale crater, Mars

Thorpe, et al., (this volume), Mars Science Laboratory CheMin data from the Glen Torridon region and the significance of lake-groundwater interactions in interpreting mineralogy and sedimentary history

References:

Achilles, C. N., Downs, R. T., Ming, D. W., Rampe, E. B., Morris, R. V., Treiman, A. H., et al. (2017), Mineralogy of an active eolian sediment from the Namib dune, Gale crater, Mars. *Journal of Geophysical Research, Planets 122*(11), doi.org/10.1002/2017JE005262

Achilles, C. N., Rampe, E. B., Downs, R. T., Bristow, T. F., Ming, D. W., Morris, R. V., et al. (2020), Evidence for multiple diagenetic episodes in ancient fluvial-lacustrine sedimentary rocks in Gale crater, Mars. *Journal of Geophysical Research, Planets* 125(8), doi:10.1029/2019JE006295

Anderson, R. B., & Bell, J. F. III (2010), Geologic mapping and characterization of Gale crater and implications for its potential as a Mars Science Laboratory landing site. *Mars 5*, 76–128. doi.org/10.1555/mars.2010.0004

Banham, S.G., Gupta, S., Rubin, D.M., Watkins, J.A., Sumner, D.Y., Edgett, K.S., et al. (2018), Ancient martian aeolian processes and palaeomorphology reconstructed from the Stimson formation on the lower slope of Aeolis Mons, Gale crater, Mars. *Sedimentology, 65*, 993–1042. doi.org/10.1111/sed.12469

Banham, S. G., Gupta, S., Rubin, D. M., Edgett, K. S., Barnes, R., Van Beek, J., et al. (2021), A rock record of complex aeolian bedforms in a Hesperian desert landscape: The Stimson formation as exposed in the Murray buttes, Gale crater, Mars. *Journal of Geophysical Research: Planets, 126* (4): e2020JE006554. doi

Bedford, C. C., Bridges J. C., Schwenzer, S. P., Wiens, R. C., Rampe, E. B., Frydenvang, J. & Gasda, P. J. (2019), Alteration trends and geochemical source region characteristics preserved in the fluviolacustrine sedimentary record of Gale crater, Mars. *Geochimica et Cosmochimica Acta, 246*, 234-266. doi.org/10.1016/j.gca.2018.11.031

Berger, J.A., R. Gellert, N.I. Boyd, P.L. King, M.A. McCraig, C.D. O'Connell-Cooper, et al., (2020), Elemental composition and chemical evolution of geologic materials in Gale crater, Mars: APXS results from Bradbury Landing to the Vera Rubin Ridge. *Journal of Geophysical Research: Planets, 12*(12), doi: 10.1029/2020JE006538

970 Bibring, J-P., Langevin, T., Mustard, J. F., Poulet, F., Arvidson, R., Gendrin, A., et al. (2006),
971 Global mineralogical and aqueous Mars history derived from OMEGA/Mars Express data.
972 *Science 312*(5772), 400-404. doi:10.1126/science.1122659

973 Blake, D.F., Vaniman, D., Achilles, C., Anderson, R., Bish, D., Bristow, T., et al. (2012),
974 Characterization and calibration of the CheMin mineralogical instrument on Mars Science
975 Laboratory. *Space Science Reviews 170*: 341-399. doi:10.1007/s11214-012-9905-1

976 Bonyadia, Z., & Sadeghib, R., (2020), Hydrothermal alteration associated with magnetite
977 mineralization in the Bafq iron deposits, Iran. *Journal of Asian Earth Sciences, 189*, 104152.
978 doi.org/10.1016/j.jseaes.2019.104152

979 Bristow, T.F., Rampe, E.B., Achilles, C.N., Blake, D.F., Chipera, S.J., Craig, P. et al. (2018),
980 Clay mineral diversity and abundance in sedimentary rocks of Gale crater, Mars. *Science*
981 *Advances, 4*(6), article ear3330, doi:10.1126/sciadv.aar3330

982 Bristow, T.F., J. P. Grotzinger, E. B. Rampe, J. Cuadros, S. J. Chipera, G. W. Downs, et al.,
983 (2021), Brine-driven destruction of clay minerals in Gale crater, Mars. *Science, 373*(6551),
984 doi:10.1126/science.abg5449

985 Bryk, A. B., Dietrich, W. E., Lamb, M. P., Grotzinger, J. P., Vasavada, A. R., Stack, K. M., et
986 al., (2019), What was the original extent of the Greenheugh pediment and Gediz Vallis ridge
987 deposits in gale crater, mars? Paper presented at *Ninth International Conference on Mars*.
988 Abstract 6296. Pasadena, California.

989 Campbell, J. L., Perrett, G. M., Gellert, R., Andrushenko, S. M., Boyd, N. I., Maxwell, J. A., et
990 al. (2012), Calibration of the Mars Science Laboratory alpha particle X-ray spectrometer. *Space*
991 *Science Reviews*, *170*, 319– 340. doi.org/10.1007/s11214-012-9873-5

992 Campbell, J. L., King, P. L., Burkemper, L., Berger, J. A., Gellert, R., Boyd, N. I., et al. (2014),
993 The Mars Science Laboratory APXS calibration target: Comparison of Martian measurements
994 with the terrestrial calibration. *Nuclear Instruments and Methods in Physics Research Section B:*
995 *Beam Interactions with Materials and Atoms*, *323*, 49– 58. doi.org/10.1016/j.nimb.2014.01.011

996 Cousin, A., Sautter, V., Payre, V., Forni, O., Mangold, N., Le Diet, L., et al. (2017),
997 Classification of igneous rocks analyzed by ChemCam at Gale Crater, Mars. *Icarus 288*, 265-
998 283. doi:10.1016/j.icarus.2017.01.014

999 Davis, K., Herman, J., Maksymuk, M., Wilson, J., Chu, P., Burke, K., Jandura, L., & Brown, K.,
1000 (2012), Mars Science Laboratory Dust Removal Tool. Paper presented at the *41st Aerospace*
1001 *Space Mechanisms Symposium*, Paper #12, Pasadena, California.

1002 Edgar, L.A., Fedo, C. M., Gupta, S., Banham, S.G., Fraeman, A.A. Grotzinger, J.P et al. (2020),
1003 A lacustrine paleoenvironment recorded at Vera Rubin ridge, Gale crater: Overview of the
1004 sedimentology and stratigraphy observed by the Mars Science Laboratory Curiosity rover.
1005 *Journal of Geophysical Research, Planets, 125*(3) doi: 10.1029/2019JE006307

1006 Edgar, L.A., Gupta, S., Rubin, D.M., Lewis, K.W., Kocurek, G.A., Anderson, R.B., et al. (2018),
1007 Shaler: *in situ* analysis of a fluvial sedimentary deposit on Mars. *Sedimentology, 65*(1):96-122,
1008 doi:10.1111/sed.12370

1009 Edgett, K. S., Yingst, R. A., Ravine, M. A., Capilinger, M. A., Maki, J. N., Ghaemi, F. T., et al.
1010 (2012), Curiosity's Mars Hand Lens Imager (MAHLI) Investigation. *Space Science Review, 170*:
1011 259. https://doi.org/10.1007/s11214-012-9910-4

1012 Edwards, P. H., Bridges, J. C., Wiens, R., Anderson, R., Dyar, D., Fisk, M., et al. (2017), Basalt–
1013 trachybasalt samples in Gale crater, Mars. *Meteoritics and Planetary Science, 52* 2931-2410.
1014 doi.org/10.1111/maps.12953

1015 Fedo, C.M., J.P. Grotzinger, A. Bryk, L.A. Edgar, K. Bennett, V. Fox, N. Stein, A. Fraeman, S.
1016 Banham, S. Gupta, K. Edgett, et al., (2020), Ground-based stratigraphic correlation of the Jura
1017 and Knockfarril Hill members of the Murray formation, Gale crater: Bridging the Vera Rubin
1018 ridge–Glen Torridon divide. Paper presented at 51st Lunar and Planetary Science Conference,
1019 Abstract # 2345, Woodlands, Texas.

1020 Fraeman, A. A., Ehlmann, B. L., Arvidson, R. E., Edwards, C. S., Grotzinger, J. P., Milliken, R.
1021 E., Quinn, D. P., & Rice, M. S. (2016), The stratigraphy and evolution of lower Mount Sharp
1022 from spectral, morphological, and thermophysical orbital data sets. *Journal of Geophysical*
1023 *Research, Planets*, *121*, 1713–1736. doi:10.1002/2016JE005095

1024 Fraeman, A.A., Edgar, L.A., Rampe, E. B., Thompson, L. M., Frydenvang, J., Fedo, C. M., et al.
1025 (2020), Evidence for a diagenetic origin of Vera Rubin ridge, Gale crater, Mars: Summary and
1026 synthesis of Curiosity's exploration campaign. *Journal of Geophysical Research Planets* doi:
1027 10.1029/2020JE006527

1028 Gellert, R., Rieder, R., Brückner, J., Clark, B.C., Dreibus, G., Klingelhöfer, G., et al. (2006),
1029 Alpha Particle X-Ray Spectrometer (APXS): Results from Gusev crater and calibration report.
1030 *Journal of Geophysical. Research, Planets*, *111*, E02S05. doi.org/10.1029/2005JE002555

1031 Gellert, R., Clark, B.C. III, & Mars Science Laboratory (MSL) Science Team (2015), In situ
1032 compositional measurements of rocks and soils with the Alpha Particle X-ray Spectrometer on
1033 NASA's Mars rovers. *Elements 11*, 39–44. https://doi.org/10.2113/gselements.11.1.39

1034 Goldich, S. S. (1938), A Study in Rock-Weathering. *The Journal of Geology*, *46* (1): 17–
1035 58. doi:10.1086/624619

1036 Grotzinger, J. P., Crisp, J., Vasavada, A. R., Anderson, R. C., Baker, C. J., Barry, R., et al.
1037 (2012), Mars Science Laboratory mission and science investigation. *Space Science Reviews*, *170*,
1038 5 – 56. doi:10.1007/s11214-012-9892-2.

1039 Grotzinger, J.P., Sumner, D. Y., Kah, L. C., Stack, K., Gupta, S., Edgar, L., et al. (2014), A
1040 habitable fluvio-lacustrine environment at Yellowknife Bay, Gale Crater, Mars. *Science*,
1041 *343*(6169), 1242777. doi:10.1126/science.1242777.

1042 Grotzinger, J. P., Gupta, S., Malin, M.C., Rubin, D.M., Schieber, J., Siebach, K., et al. (2015),
1043 Deposition, exhumation, and paleoclimate of an ancient lake deposit, Gale Crater, Mars. *Science*,
1044 *350*(6257), aac7575. doi:10.1126/science.aac7575.

1045 Hausrauth, E. M., Ming, D. W., Peretyazhko, T. S., & Rampe, E. B., (2018) Reactive transport
1046 and mass balance modeling of the Stimson sedimentary formation and altered fracture zones
1047 constrain diagenetic conditions at Gale crater, Mars. Earth and Planetary Science Letters, 491, 1-
1048 10. doi.org/10.1016/j.epsl.2018.02.037

1049 Hudson, B.D., (1995), Reassessment of Polynov's ion mobility series. Soil Science Society of
1050 America Journal, 59, 1101-1103. doi.org/10.2136/sssaj1995.03615995005900040022x

1051 Hurowitz, J. A., Grotzinger, J. P., Fischer, W. W., McLennan, S. M., Milliken, R. E., Stein, N., et
1052 al. (2017), Redox stratification of an ancient lake in Gale crater, Mars. *Science, 356*, eaah6849

1053 Hughes, M. N., Arvidson, R. E., Bryk, A. B., Dietrich, W. E., Lamb, M. P., & Catalano, J. G.,
1054 (2020), Mass Movements and Debris Deposits in the Grand Canyon and Gediz Vallis, Gale
1055 Crater, Mars. Paper presented at *51st Lunar and Planetary Science Conference*, Abstract #2426,
1056 Woodlands, Texas.

1057 Klimchouck, A., (1996), The dissolution and conversion of gypsum and anhydrite. *International*
1058 *Journal of Speleology 25* (3-4), 21-36. doi.org/10.5038/1827-806X.25.3.2

1059 Kronyak, R.E., Kah, L.C., Edgett, K.S., VanBommel, S.J., Thompson, L.M., Wiens, R.C., Sun,
1060 V.Z., & Nachon, M. (2019), Mineral-filled fractures as indicators of multigenerational fluid flow
1061 in the Pahrump Hills member of the Murray formation, Gale crater, Mars. *Earth and Space*
1062 *Science, 6*, 238–265. https://doi.org/10.1029/2018EA000482

1063 Mahaffy, P. R., Webster, C. R., Cabane, M., Conrad, P. G., Coll, P., Atreya, S. K., et al. (2012),
1064 The sample analysis at Mars investigation and instrument suite. *Space Science Reviews, 170*(1-
1065 4), 401-478.

1066 Malin, M.C., & Edgett. K.S., (2000), Sedimentary rocks of early Mars. *Science, 290*, 1927-
1067 1937. doi: 10.1126/science.290.5498.1927

1068 Malin, M.C., Ravine, M.A. Caplinger, M.A. Ghaemi, F.T. Schaffner, J.A. Maki, J.N., et al.
1069 (2017), The Mars Science Laboratory (MSL) Mast cameras and Descent imager: Investigation
1070 and instrument descriptions. *Earth and Space Science, 4*(8):506-539,
1071 doi:10.1002/2016EA000252

1072 Mc Lennan, S. M., (2003), Sedimentary silica on Mars. Geology 31:315–318. doi:10.1130/0091-
1073 7613

1074 Mc Lennan, S. M., Grotzinger, J. P., Hurowitz, J. A., & Tosca, N., J., (2019), The sedimentary
1075 cycle on early Mars. *Annual Review of Earth and Planetary Sciences, 47*: 91-118,
1076 doi.10.1146/annurev-earth-053018- 060332

1077 Milliken, R. E., Grotzinger, J. P., & Thomson, B. J. (2010), Paleoclimate of Mars as captured by
1078 the stratigraphic record in Gale Crater. *Geophysical Research Letters*, *37*(4), L04201.
1079 doi:10.1029/2009GL041870

1080 Milliken, R.E., Ewing, R.C., Fischer, W.W., and Hurowitz, J., (2014), Wind-blown sandstones
1081 cemented by sulfate and clay minerals in Gale Crater, Mars. *Geophysical Research Letters, v. 41*,
1082 p. 1149– 1154, doi.org/10.1002/2013GL059097.

1083 Nesbitt, H.W., & Wilson, R.E. (1992), Recent chemical weathering of basalt. *American Journal*
1084 *of Science, 292*, 740–777.

1085 Nesbitt, H. W., & Young, G. M. (1982), Early Proterozoic climates and plate motions inferred
1086 from major element chemistry of lutites. *Nature, 299*(5885), 715–717. doi.org/10.1038/299715a0

1087 O'Connell-Cooper, C.D., Spray, J.G., Thompson, L.M., Gellert, R., Berger, J.A., Boyd, N.I., et
1088 al. (2017), APXS-derived chemistry of the Bagnold dune sands: Comparisons with Gale Crater

soils and the global Martian average. *Journal of Geophysical Research Planets, 122*(12):2623-2643, doi:10.1002/2017JE005268

Palucis, M. C., Dietrich, W. E., Hayes, A. G., Williams, R. M., Gupta, S., Mangold, N., et al., (2014), The origin and evolution of the Peace Vallis fan system that drains to the Curiosity landing area, Gale Crater, Mars. *Journal of Geophysical Research Planets 119*(4): 705-728, doi.org/10.1002/2013JE004583

Rampe, E.B., Ming, D.W., Blake, D.F., Bristow, T.F., Chipera, S.J., Grotzinger, J.P., et al. (2017), Mineralogy of an ancient lacustrine mudstone succession from the Murray formation, Gale crater, Mars. *Earth and Planetary Science Letter,s 471*, 172– 158. doi.org/10.1016/j.epsl.2017.04.021

Rampe, E.B., Lapotre, M. G. A., Bristow, T.F., Arvidson, R. E., Morris, R. V., Achilles, C. N., et al. (2018), Sand mineralogy within the Bagnold dunes, Gale crater, as observed in situ and from orbit. Geophysical Research Letters, 45(18), 9488-9497. doi.org/10.1029/2018GL079073

Rampe, E. B., Bristow, T. F., Morris, R. V., Morrison, S. M., Achilles, C. N., Ming, D. W., et al. (2020a), Mineralogy of Vera Rubin Ridge from the Mars Science Laboratory CheMin Instrument. *Journal of Geophysical Research-Planets*. doi:10.1029/2019JE006306

Rampe, E. B., Blake, D.F., Bristow, T. F., Ming, D. W., Vaniman, D. T., Morris, R. V., et al. (2020b), Mineralogy and geochemistry of sedimentary rocks and eolian sediments in Gale crater, Mars: A review after six Earth years of exploration with Curiosity. *Geochemistry, 80*(2). doi:10.1016/j.chemer.2020.125605

Rampe, E. B., Yen, A., Bristo, T, Blake D. F., Vaniman, D. , Achilles, C. N., et al. (2020c), Mineralogy of the Greenheugh Pediment and Underlying Murray Formation from the Mars Science Laboratory CheMin Instrument. Paper presented at *American Geophysical Union Fall Meeting, December 2020*. Abstract P070-09.

Rieder, R., Gellert, R., Brückner, J., Klingelhöfer, G., Dreibus, G., Yen, A. & Squyres, S. W. (2003), The new Athena alpha particle X-ray spectrometer for the Mars Exploration Rovers. *Journal of Geophysical Research, Planets, 108*, E12, 8066. https://doi.org/10.1002/2015GL066675

Sautter, V., Toplis, M. J., Wiens, R. C., Cousin, A., Fabre, C., & Gasnault, O. (2015), In situ evidence for continental crust on early Mars. *Nature Geoscience, 8*(8), 605.

Schieber, J., et al., (2017), Encounters with an unearthly mudstone: Understanding the first mudstone found on Mars. *Sedimentology, 64*, p. 311-358. doi:10.1111/sed.12318.

Schmidt, M. E., Campbell, J. L., Gellert, R., Perrett, G. M., Treiman, A. H., Blaney, D. L. et al. (2014), Geochemical diversity in first rocks examined by the Curiosity rover in Gale crater: Evidence for and significance of an alkali and volatile-rich igneous source, *Journal of Geophysical Research Planets*, *119*(1):64-81, doi:10.1002/2013JE004481

Stack, K.M., Grotzinger, J.P., Lamb, M.P., Gupta, S., Rubin, D.M., Kah, L.C., et al. (2019), Evidence for plunging river plume deposits in the Pahrump Hills member of the Murray formation, Gale crater, Mars. *Sedimentology 66*, 1768–1802. https://doi.org/10.1111/sed.12558

Stein, N.T., Quinn, D.P., Grotzinger, J.P., Fedo, C., Ehlmann, B.L., Stack, K. M., et al. (2020), Regional structural orientation of the Mt. Sharp group revealed by in-situ dip measurements and

stratigraphic correlations on the Vera Rubin ridge. *Journal of Geophysical Research, Planets, 125*(5), doi: 10.1029/2019JE006298

Stolper, E. M., Baker, M. B., Newcombe, M. E., Schmidt, M. E., Treiman, A. H., Cousin, A., et al. (2013), The petrochemistry of Jake M: A martian mugearite. *Science 341* (6153), 1239463. doi:10.1126/science.1239463

Sutter, B., McAdam, A.C., Archer, P. D., Ming, D.W., Eigenbrode, J. L., Rampe, E.B., et al. (2020), Geochemical Processes Along and Above the Glen Torridon/Greenheugh Pediment, Unconformity, Gale Crater, Mars: Results from the Sample Analysis at Mars Instrument. Paper presented at *American Geophysical Union Fall Meeting, December 2020*. Abstract P070-07

Thomson, B. J., Bridges, N. T., Milliken, R., Baldridge, A., Hook, S. J., Crowley, J. K., et al. (2011), Constraints on the origin and evolution of the layered mound in Gale Crater, Mars using Mars Reconnaissance Orbiter data. *Icarus*, *214*(2), 413–432. doi.org/10.1016/j.icarus.2011.05.002

Thompson, L. (2020), Alpha Particle X-ray spectrometer geochemistry of the Murray formation and Vera Rubin ridge, Gale crater, Mars. https://doi.org/10.25545/ZXDJZ7, UNB, V1, UNF:6:bL/a2qTZBu6DNJlzkmGAbg==[fileUNF]

Thompson, L. (2022) Alpha Particle X-ray spectrometer geochemistry of rocks associated with the Basal Siccar Point group unconformity, Glen Torridon region, Gale crater, Mars. doi to be supplied upon final submission

Thompson, L. M., J.A. Berger, J.G. Spray, A.A. Fraeman, M.A. McCraig, C.D. O'Connell-Cooper, et al., (2020), APXS-derived compositional characteristics of Vera Rubin Ridge and Murray formation, Gale crater, Mars: Geochemical implications for the origin of the ridge. *Journal of Geophysical Research: Planets, 125*(10), doi: 10.1029/2019JE006319

Thompson, L. M., Schmidt, M. E., Spray, J. G., Berger, J. A., Fairén, A. G., Campbell J. L., et al. (2016), Potassium-rich sandstones within the Gale impact crater, Mars: The APXS perspective. *Journal of Geophysical Research Planets, 121*(10):1981-2003, doi:10.1002/2016JE005055

Treiman, A. H., Bish, D. L., Vaniman, D. T., Chipera, S. J., Blake, D. F., Ming, D. W., et al. (2016), Mineralogy, provenance and diagenesis of a potassic basaltic sandstone on Mars: CheMin X-ray diffraction of the Windjana sample (Kimberley area, Gale Crater). *Journal of Geophysical Research, 121*(1), p.75 – 106. doi:10.1002/2015JE004932

VanBommel, S.J., Gellert, R., Berger, J.A., Campbell, J.L., Thompson, L.M., Edgett, K.S., et al. (2016), Deconvolution of distinct lithology chemistry through oversampling with the Mars Science Laboratory Alpha Particle X-ray Spectrometer. *X-Ray Spectrometry, 45*, 155–161. https://doi.org/10.1002/xrs.2681

VanBommel, S.J., Gellert, R., Berger, J.A., Thompson, L.M., Edgett, K.S., McBride, M.J., et al. (2017), Modeling and mitigation of sample relief effects applied to chemistry measurements by the Mars Science Laboratory Alpha Particle X-ray Spectrometer. *X-Ray Spectrometry, 46*, 229–236. https://doi.org/10.1002/xrs.2755

VanBommel, S.J., Gellert, R., Boyd, N.I., & Hanania, J.U. (2019), Empirical simulations for further characterization of the Mars Science Laboratory Alpha Particle X-ray Spectrometer: An Introduction to the ACES program. *Nuclear Instrumentation and Methods, B 441*, 79–87. https://doi.org/10.1016/j.nimb.2018.12.040

Watkins, J. A., Grotzinger, J., Stein, N., Banham, S. G., Gupta, S., Rubin, D., Stack, K. M., Edgett, K. S., (2016), Paleotopography of Erosional Unconformity, Base of Stimson Formation, Gale Crater, Mars. Paper presented at the *47th Lunar and Planetary Science Conference*, Abstract #2939, Woodlands, Texas

Williams, R.M.E., Grotzinger, J.P., Dietrich, W.E., Gupta, S., Sumner, D.Y., Wiens, R.C., et al. (2013), Martian fluvial conglomerates at Gale crater. *Science 340*, 10681072. https://doi.org/10.1126/science.1237317

Wiens, R. C., et al., (2020), Origin and composition of three heterolithic boulder- and cobble-bearing deposits overlying the Murray and Stimson formations, Gale Crater, Mars. *Icarus, 350*, 113897. doi.org/10.1016/j.icarus.2020.113897

Yen, A.S., Ming, D.W., Vaniman, D.T., Gellert, R., Blake, D.F., Morris, R.V., et al. (2017), Multiple stages of aqueous alteration along fractures in mudstone and sandstone strata in Gale crater, Mars. *Earth and Planetary Science Letters,* 471, 186–198. doi:10.1016/j.epsl.2017.04.033

Yen, A.S., Morris, R.V., Ming, S.P., Schwenzer, Sutter, B., D.W., Vaniman, et al. (2021), Formation of tridymite and evidence for a hydrothermal history at Gale crater, Mars. *Journal of Geophysical Research Planets*, *126*, e2020JE006569. doi:1.1029/2020JE006569

Supporting Information References

Brimhall, G. H., & Dietrich, W. E. (1987), Constitutive mass balance relations between chemical composition, volume, density, porosity, and strain in metasomatic hydrochemical systems: results on weathering and pedogenesis. *Geochimica et Cosmochimica Acta, 51*(3), 567–587.